Open access • Posted Content • DOI:10.1101/2021.02.21.21252137

Evolving Infection Paradox of SARS-CoV-2: Fitness Costs Virulence? — Source link

A. S. M. Rubayet Ul Alam, Ovinu Kibria Islam, Md. Shazid Hasan, Mir Raihanul Islam ...+6 more authors

Institutions: Jessore University of Science & Technology, BRAC University, University of Rajshahi, George Washington University ...+1 more institutions

Published on: 23 Feb 2021 - medRxiv (Cold Spring Harbor Laboratory Press)

Topics: Viral evolution, Mutation, Viral load, Virulence and Epistasis

Dominant Clade-featured SARS-CoV-2 Co-occurring Mutations Reveals Plausible Epistasis: An *in silico* based Hypothetical Model

A. S. M. Rubayet Ul Alam[1#], Ovinu Kibria Islam[1#], Md. Shazid Hasan[1], Mir Raihanul Islam[2], Shafi Mahmud[3], Hassan M. Al Emran[4], Iqbal Kabir Jahid[1], Keith A. Crandall[5], M. Anwar Hossain[6,7*]

1 Department of Microbiology, Jashore University of Science and Technology, Jashore-7408, Bangladesh

2 BRAC James P Grant School of Public Health, BRAC University, Bangladesh

3 Genetic Engineering and Biotechnology, University of Rajshahi, Rajshai-6205, Bangladesh

4 Department of Biomedical Engineering, Jashore University of Science and Technology, Jashore-7408, Bangladesh

5 Computational Biology Institute and Department of Biostatistics & Bioinformatics, Milken Institute School of Public Health, The George Washington University, Washington, DC, USA

6 Jashore University of Science and Technology, Jashore-7408, Bangladesh

7 Department of Microbiology, University of Dhaka, Dhaka-1000, Bangladesh

***Correspondence**

M. Anwar Hossain, Jashore University of Science and Technology, Jashore-7408, Bangladesh.

E-mail: hossaina@du.ac.bd, Contact: +8801715363753

 # Authors contributed equally

ABSTRACT

SARS-CoV-2 is evolved into eight fundamental clades where four (G, GH, GR, and GV) are globally prevalent in 2020. How the featured co-occurring mutations of these clades are linked with viral fitness is the main question here and we thus proposed a hypothetical model using *in silico* approach to explain the plausible epistatic effects of those mutations on viral replication and transmission. Molecular docking and dynamics analyses showed the higher infectiousness of a spike mutant through more favorable binding of G_{614} with the elastase-2. RdRp mutation p.P323L significantly increased genome-wide mutations ($p<0.0001$) since more flexible RdRp (mutated)-NSP8 interaction may accelerate replication. Superior RNA stability and structural variation at NSP3:C241T might impact protein and/or RNA interactions. Another silent 5'UTR:C241T mutation might affect translational efficiency and viral packaging. These four G-clade-featured co-occurring mutations might increase viral replication. Sentinel GH-clade ORF3a:p.Q57H constricted ion-channel through inter-transmembrane-domain interaction of cysteine(C81)-histidine(H57) and GR-clade N:p.RG203-204KR would stabilize RNA interaction by a more flexible and hypo-phosphorylated SR-rich region. GV-clade viruses seemingly gained the evolutionary advantage of the confounding factors; nevertheless, N:p.A220V might modulate RNA binding with no phenotypic effect. Our hypothetical model needs further retrospective and prospective studies to understand detailed molecular events featuring the fitness of SARS-CoV-2.

Key words

SARS-CoV-2, COVID-19, Infection Paradox, Fitness, Virulence, Clades, Co-occurring mutations

1. Introduction

Severe acute respiratory syndrome coronavirus 2 (SARS-CoV-2), the etiological agent of COVID-19 pandemic, has gained some extraordinary attributes that make it extremely infectious: High replication rate, large burst size, high stability in the environment, strong binding efficiency of spike glycoprotein (S) receptor-binding domain (RBD) with human angiotensin-converting enzyme 2 (ACE2) receptor, and additional furin cleavage site in S protein[1-3]. In addition to those, it has proofreading capability ensuring relatively high-fidelity replication[4]. The virus contains four major structural proteins: spike glycoprotein (S), envelope (E), membrane (M), and nucleocapsid (N) protein along with 16 nonstructural proteins (NSP1 to NSP16) and seven accessory proteins (ORF3a, ORF6, ORF7a, ORF7b, ORF8a, ORF8b, and ORF10)[5,6]. Mutational spectra within the SARS-CoV-2 genome[7,8], spike protein[9], RdRp[10], ORF3a[11], and N protein[12] were reported.

SARS-CoV-2 was classified into eight major clades, such as G, GH, GR, GV, S, V, L, and O by global initiative on sharing all influenza data (GISAID) consortium (https://www.gisaid.org/) based on the dominant core mutations in genomes where four clades (G, GH, GR, and GV) are globally and geographically prevalent in 2020[13]. Yin [14] reported that the 5′UTR mutation 241C > T is co-occurring with three other mutations, 3037C > T (NSP3: C318T), 14408C > T (RdRp: p.P323L), and 23403A > G (S: p.D614G). GISAID referred to these co-occurring mutations containing viruses as clade G (named after the spike D614G mutation) or PANGO (https://cov-lineages.org/) lineage B.1[15,16]. The GR clade or lineage B.1.1.* is classified with additional trinucleotide mutations at 28881-28883 (GGG>AAC); creating two consecutive amino acid changes, R203K and G204R, in N protein. Another derivative of G clade is GH or lineage B.1.*, characterized by an additional ORF3a:p.Q57H mutation. The variant GV or lineage B.1.177 featured an A222V mutation in the S protein along with other mutations of the clade G[13,16]. Also, N: A220V, ORF10: V30L and three other synonymous mutations T445C, C6286T, and C26801G are observed for this clade[17].

The most frequently observed mutation is D614G of the S protein[18], which has direct roles in receptor binding, and immunogenicity, thus viral immune-escape, transmission, and

replication fitness[19,20]. Mutations in proteins other than spike could also affect viral pathogenicity and transmissibility, but the role of those dominant clade-featured mutations has remained largely underestimated. Although the possible role of ORF3a:p.Q57H in replication cycle[21] has recently been investigated, the molecular perspective was not fully explained there. The effect of 5'UTR: C241T, Leader: T445C, NSP3: C318T, RdRp:p.P323L, N:p.RG203-203KR, and N:p.A220V is still being overlooked.

Different mutation(s) of SARS-CoV-2 may work independently or through epistatic interactions[22,23]; however, it is difficult to determine exactly how these co-occurring mutations, if not all, might have gained their selective evolutionary fitness[22,24,25]. Hence, many hypothetical questions remain: What are the impacts of these mutations on protein structures, and what can be their functional roles? How might these mutated proteins interact together? Is there any possible role of the co-occurring 'silent' mutation? Could these mutations have any plausible impact on viral fitness and virulence? We attempt here to answer these questions by *in silico* molecular insights of SARS-CoV-2 mutants and possible interactions of proteins containing co-occurring mutations. Overall, this study aims to determine plausible individual and/or epistatic impacts of those mutants during replication in terms of viral entry and fusion, evasion of host cell lysis, replication rate, ribonucleoprotein stability, protein-protein interactions, translational capacity, and ultimately the probable combined effect on viral transmission and fitness.

2. Materials and Methods

2.1 Retrieval of Sequences and Mutation Analyses

This study analyzed 225,526 high-coverage (<1% Ns and <0.05% unique amino acid mutations) and complete (>29,000 nucleotides) genome sequences from a total of 3,16,166 sequences submitted to GISAID from January 01, 2020, to January 03, 2021. We removed the non-human host-generated sequences during dataset preparation. The Wuhan-Hu-1 (Accession ID- NC_045512.2) isolate was used as the reference genome.

A python script (https://github.com/hridoy04/counting-mutations) was used to partition a significant part of the dataset into two subsets based on the RdRp: C14408T mutation and estimated the genome-wide variations (single nucleotide changes) for each strain. For the genome-wide mutation analysis, a total of 37,179 sequences (RdRp wild type or 'C' variant: 9,815; and mutant or 'T' variant: 27,364) were analyzed from our dataset. The frequency of

mutations was tested for significance with the Wilcoxon signed-rank test between RdRp 'C' variant and 'T' variant using IBM SPSS statistics 25.

2.2 Stability, Secondary and Three-Dimensional Structure Prediction Analyses of S, RdRp, ORF3a, and N Proteins

DynaMut[26] and FoldX 5.0[27,28] were used to determine the stability of both wild and mutant variants of N, RdRp, S, and ORF3a proteins. PredictProtein[29] was utilized for analyzing and predicting the possible secondary structure and solvent accessibility of both wild and mutant variants of those proteins. The SWISS-MODEL homology modeling webtool[30] was utilized for generating the three-dimensional (3D) structures of the RdRp, S, and ORF3a protein using 7c2k.1.A, 6xr8.1.A, and 6xdc.1.A PDB structure as the template, respectively. Modeller v9.25[31] was also used to generate the structures against the same templates. I-TASSER[32] with default protein modeling mode was employed to construct the N protein 3D structure of wild and mutant type since there was no template structure available for the protein. The built-in structural assessment tools (Ramachandran plot, MolProbity, and Quality estimate) of SWISS-MODEL were used to check the quality of generated structures.

2.3 Molecular Docking and Dynamics of RdRp-NSP8 and Spike-Elastase2 Complexes

Determination of the active sites affected by binding is a prerequisite for docking analysis. We chose 323 along with the surrounding residues (315-324) of RdRp and the residues 110 to 122 of NSP8 monomer as the active sites based on the previously reported structure[33]. The passive residues were defined automatically where all surface residues were selected within the 6.5°A radius around the active residues. The molecular docking of the wild and predicted mutated RdRp with the NSP8 monomer from the PDB structure 7C2K was performed using the HADDOCKv2.4 to evaluate the interaction[34]. The binding affinity of the docked RdRp-NSP8 complex was predicted using the PRODIGY[35]. The number and specific interfacial contacts (IC) for each of the complexes were identified.

The human neutrophil elastase (hNE) or elastase-2 (PDB id: 5A0C) was chosen for docking of the S protein, based on earlier reports[36]. Here we employed CPORT[37] to find out the active and passive protein-protein interface residues of hNE. The S protein active sites were chosen based on the target region (594-638) interacting with the elastase-2. The passive residues of S protein were defined automatically as mentioned for RdRp-NSP8 docking analysis. Afterward, we individually docked wild (614D) and mutated (614G) S protein with

the hNE using HADDOCK 2.4. The binding affinity of the docked complexes, as well as the number and specific interfacial contacts (IC), were predicted as performed after RdRP-NSP8 docking. We employed HDOCK server[38] with specifying the active binding sites residues for predicting the molecular docking energy.

The structural stability of the above-mentioned protein complexes (RdRP-NSP8 and Spike-Elastase2) and their variations were assessed through YASARA Dynamics software package (Land & Humble, 2018). We used AMBER14 force field (Dickson et al., 2014) for these four systems, and the cubic simulation cell was created with the TIP3P (at 0.997 g/L-1, 25C, and 1 atm) water solvation model. The PME or particle mesh Ewald methods were applied to calculate the long-range electrostatic interaction by a cut-off radius of 8Å[39]. We applied the Berendsen thermostat to maintain the temperature of the simulation cell. The time step of the simulation was set as 1.25fs[40] and the simulation trajectories were saved after every 100ps. Finally, we conducted the molecular dynamics simulation for 100ns[41-44].

2.4 Mutational Analysis of Transmembrane Domain 1 of ORF3a and serine-rich (SR) domain of N protein

The complete genome of 12 pangolin-derived coronavirus strains, as well as 38 bats, civet, and human SARS-CoVs, were downloaded from GISAID and NCBI, respectively for the mutational comparison between the SARS-CoV and SARS-CoV-2. We mainly targeted transmembrane domain 1 (TM1), which covers 41 to 63 residues, of ORF3a to find the identical mutation and scan overall variation in TM1. A generalized comparison between SARS-CoV and SARS-CoV-2 reference sequences was performed to identify the mutations in the SR-rich region that will help to postulate on N protein functions of novel coronavirus based on previous related research on SARS-CoV.

2.5 Analyzing RNA Folding prediction of 5´UTR, Leader protein, and NSP3

The Mfold web server[45] was used with default parameters to check the folding pattern of RNA secondary structure in the mutated 5´UTR, synonymous leader (T445C), and NSP3 region (C3037T). The change C6286T is in between the nucleic acid-binding (NAB) domain and betacoronavirus specific marker (βSM) domain of the NSP3 region. The change C26801G is at the transmembrane region 3 (TM3) of the virion membrane. Thus, changing in C6286T and C26801G will not affect the function significantly and was not predicted here. The structure of complete mutant 5´UTR (variant 'T') was compared with the wild type (variant 'C') secondary pattern as mentioned in the Huston et al. (2021) [46]. From the Mfold

web server, we also estimated free energy change (ΔG) for wild and mutant leader and NSP3 RNA fold to find any variation in stability.

3. RESULTS AND DISCUSSION

. The possible individual effects of a total nine mutations in S, RdRp, ORF3a, N, 5'UTR, leader protein (NSP1), and NSP3 in viral replication cycle and transmission were discussed with associated results. Zeng et al. (2020) showed the links of these mutations towards possible epistatic effects on fitness using statistical analysis that duly suits our purpose of presenting how the mutations might play the combined roles[23]. Whereas researches on molecular docking of the spike protein[47,48] and RdRp[49,50] in search of potential drug targets is a continuous process, our study approached in a unique way to dock spike with elastase-2 and RdRp with NSP8 to satisfy our purposes. The overall epistatic interactions of the mutant proteins and/or RNA was then depicted (Figure 1) as a hypothetical model and discussed.

3.1 Spike Protein D614G Mutation Favors Elastase-2 Binding

This study found interesting structural features of the S protein while comparing and superimposing the wild protein (D_{614}) over mutated protein (G_{614}). The secondary structure prediction and surface accessibility analyses showed that there was a slight mismatch at the S1-S2 junction (^{681}PRRAR↓S^{686}) where serine at 686 (S^{686}) was found covered in G_{614} and exposed to the surface in D_{614}. However, S^{686} in both G_{614} and D_{614} were exposed to an open-loop region to have possible contact with the proteases (supplementary Figure S1). Further investigation on the aligned 3D structures however showed no conformational change at the S1-S2 cleavage site (Figure 2c). We also observed no structural variation in the surrounding residues of the protease-targeting S1-S2 site (Figure 2c), which eliminated the assumption of Phan[51]. The predictive 3D models and structural assessment of D_{614} and G_{614} variants confirmed that the cleavage site at 815-16 of S2 subunit (^{812}PSKR↓S^{816}) or S2'[1,52] had no structural and surface topological variation (Figure 2d-e). Rather, the superimposed 3D structures suggested a conformational change in the immediate downstream region (^{618}TEVPVAIHADQLTPT^{632}) of the 614th position of mutated protein (G_{614}) that was not observed in D_{614} variants (Figure 2a-b).

Several experiments suggested that mutated (G_{614}) protein contains a novel serine protease cleavage site at 615-616 that is cleaved by host elastase-2, a potent neutrophil elastase, level of which at the site of infection during inflammation will facilitate the host cell entry for G_{614}[18,36,53,54]. The elastase-2 restrictedly cut valine at 615, due to its valine-

dependent constriction of catalytic groove[55]. The present sequence setting surrounding G_{614} (P6-^{610}VLYQGV↓NCTEV^{620}-P'5) showed a higher enzymatic activity on the spike[36] , which cannot be completely aligned with the previous works on the sequence-based substrate specificity of elastase-2[56]. However, the first non-aligned residue of the superimposed G_{614}, located at the P'4 position (T^{618}), may also be important for binding with the elastase-2, and further down the threonine (T) at 618, the residues may affect the bonding with the respective amino acids of elastase-2 (Figure 2a-b). This changed conformation at the downstream binding site of G_{614} may help overcome unfavorable adjacent sequence motifs around G^{614} residue. Therefore, the simultaneous or sequential processing of the mutated S protein by TMPRSS2/Furin/Cathepsin and/or elastase-2 facilitates a more efficient SARS-CoV-2 entry into the host cells and cell-cell fusion[36,53,54].

This study further observed the possible association of the S protein with elastase-2 and found an increased binding affinity in case of G_{614} (Table 1). Hence, the active sites of the mutated protein interacted efficiently with more amino acids of elastase-2 (Table 2), possibly providing a better catalytic activity as shown by Hu et al. (2020)[36]. The mutation may have changed the structural configuration of the elastase-2 cleavage site in a way that the enzyme is facing less challenge to get near to the cutting site of the altered protein (Figure 2a-b and 3). The efficient cleaving of this enzyme, although located in an upstream position of the S1-S2 junction, may assist in releasing S1 from S2 and change the conformation in a way that later help in cleaving at the S2' site by other protease(s) before fusion[57,58]. Mutated spike protein and elastase-2 complex was more flexible than the wild spike-elastase complex, and the interactions with enzyme was also different as shown in RMSD deviation between the complexes (Figure 4).

This G^{614} amino acid replacement may have a destabilization effect on the overall protein structure (Table 2 and Figure 2a-b). The deformed flexible region at or near G^{614} is the proof of that destabilizing change (Figure 2f and supplementary figure S3). Zhang et al.[59] explained less S1 shedding through more stable hydrogen bonding between Q^{613} (glutamine) and T^{859} (threonine) of protomer due to greater backbone flexibility provided by G^{614}. Moreover, G614 mutation may increase S protein stability and participate in N-linked glycosylation at N616[36]. On the other hand, increasing the number of RBD up conformation or increasing the chance of 1-RBD-up conformation due to breakage of both intra-and inter-protomer interactions of the spike trimer and symmetric conformation will give a better chance to bind with ACE2 receptor and can also increase antibody-mediated neutralization[60].

The S1 will release from S2 more effectively in G_{614} protein by introducing glycine that will break hydrogen bond present in between the D^{614} (wild) and T^{859} (threonine) of the neighboring protomer[60,61]. Our analyses have provided the *in silico* proof of this later fact by showing that the mutated protein was more flexible than the wild type protein by missing a hydrophobic interaction between G^{614} and Phe^{592} (Figure 2g-h). This new adjunct result accorded well with Weismann et al. (2020) that G^{614} will increase overall flexibility of the mutated protein. The overall structural change may assist the mutated S protein by providing elastase-2 a better binding space and attachment opportunity onto the cleavage site (Figure 3a-b), thus providing a more stable interaction that increases the credibility of an efficient infection (Figure 1).

3.2 Increased Flexibility of RdRp-NSP8 Complex: Compromise Proof-Reading Efficiency with Replication Speed

The binding free energy (ΔG) of the RdRp-NSP8 complexes have been predicted to be -10.6 and -10.5 $Kcalmol^{-1}$, respectively, in wild (P_{323}) and mutated (L_{323}) type that suggests a more flexible interaction for the mutated protein (Table 2). The increased number of contacts found in the L_{323}-NSP8 complex (Table 1) were possibly due to slightly more hydrogen bonds, which had no considerable impact on protein flexibility (Figure 4d). Our analyses identified that proline (P^{323}) or leucine (L^{323}) of RdRp can interact with the aspartic acid (D^{112}), cysteine (C^{114}), valine (V^{115}), and proline (P^{116}) of NSP8 (Table 1 and Figure 5). RdRp binds with NSP8 in its interface domain (from residues alanine:A^{250} to arginine:R^{365}), forming positively charged or comparatively neutral 'sliding poles' for RNA exit, and enhance the replication speed probably by extending the RNA-binding surface in that domain area[62,63]. Molecular dynamics of the mutated RdRp-NSP8 complex supported this by showing a more expanded surface area in the interacting site (Figure 4b) and maintained integrity throughout the simulation (Figure 4c). Besides, we did not find any interaction of NSP8 with the zinc-binding residues (H^{295}, C^{301}, C^{306} and C^{310}) of the RdRp protein (Table 3 and Figure 5)[64,65]. Therefore, the P323L mutation within this conserved site of the RdRp interface domain may only affect the RdRp-NSP8 interaction without changing metal binding affinity.

The results from six state-of-the-art tools of protein stability suggested that mutated (L_{323}) protein cannot be concluded as 'stable', only because of ambiguous ΔΔG estimates (Table 2), rather the interaction with the adjacent amino acid mainly defined the stability[66]. The superimposed 3D structures and secondary structure analyses showed that there was no

deviation in loop/turn structure of mutated protein, even though hydrophobic leucine (L^{323}) was embedded (supplementary Figure S1 and S4). To some extent, the mutation stabilized the L_{323} structure making the protein more rigid and binds less strongly with the NSP8 by expanding the interacting region. These variations may together increase the replication speed by helping exit the processed RNA genome from the RdRp groove structure more swiftly (Figure 1). The increasing replication speed might be due to the perturbation of interaction between RdRp and NSP8[62,66], or less possibly, the complex tripartite interactions (RdRp, NSP8, and NSP14) responsible for the speculated decrease of proof-reading efficiency[4]. Thus, RdRp mutants might increase the mutation rate by a trade-off between high replication speed and low fidelity of the mutated polymerase[67]. Another possibility could be the lower proof-reading efficiency of NSP14 that was however not linked to the replication speed[4]. Analysis of our study sequences revealed that the frequency of mutation (median=8) in L_{323} mutants (n=27,364) is significantly higher ($p<0.0001$) than the frequency (median=6) of wild-type (P_{323}) strains (n=9,815). This increased mutation rate may play a vital role in genetic drifts and provide next generations a better adaptation to adverse environments.

3.3 Q57H Substitution in ORF3a Viroporin: The Roles of Decreased Ion Permeability

This study has found that the replacement of glutamine (Q^{57}) with positively charged histidine (H^{57}) at 57 position of ORF3a transmembrane region 1 (TM1) does not change secondary transmembrane helical configuration (supplementary Figure S1), and aligned 3D structures have also shown no variation of TM1 in the monomeric state (Figure 6a). The mutant (H_{57}) protein has a non-significant increase in structural stabilization and a minimal decrease in molecular flexibility (Table 2 and supplementary Figure S5). This is because of the weak ionic interaction of H^{57}-C_α with the sulfur atom of cysteine (C^{81}) that is present in TM2 and the hydrogen bond of terminal N_ζ of lysine (K^{61}) with one of the endocyclic nitrogens of H^{57} (Figure 6b). The Q^{57} in wild-type protein forms the major hydrophilic constriction within the ORF3a channel pore[68]. Thus, further favorable increasing constrictions within the H_{57} protein channel pore due to diagonal H^{57} (TM1)-C^{81} (TM2) ionic interaction (Figure 6b) and the replacement of charge-neutral glutamine with a positively charged histidine in the selectivity filter may reduce the passing of positive ions, such as Ca^{2+}, Na^{+}, and K^{+}, by either electrostatic repulsion or blocking[69-72]. This speculation for ORF3a mutated protein was supported by another study showing the reduction of ion permeability of Na^{2+} and Ca^{2+} through the H_{57}, however, that decrease was not found statistically significant ($p>0.05$)[68].

The decrease intracellular concentration of cytoplasmic Ca^{2+} ions potentially reduces caspase-dependent apoptosis of the host cell[73], mainly supporting viral spread without affecting replication[21] as shown in Figure 1. Moreover, the ORF3a can drive necrotic cell death[74] wherein the permeated ions into cytoplasm[75] and the insertion of ORF3a as viroporin into lysosome[76] play vital roles. The H_{57} mutant may thus decrease pathogenicity and symptoms during the early stages of the infection, i.e., reducing 'cytokine storm' in the host[77]. Besides, ORF3a was proved to affect inflammasome activation, virus release, and cell death, as shown by Castaño-Rodriguez et al. (2018)[78] that the deletion of ORF3a reduced viral load and morbidity in animal models.

Even though similar proteins of ORF3a have been identified in the sarbecovirus lineage infecting bats, pangolins, and humans[79], only one pangolin derived strain from 2017 in Guangxi, China contains H^{57} residue as shown by mutation analyses (supplementary Figure S5), and also reported by Kern et al. (2020)[68]. The presence of this mutation in pangolin could be an accidental case or might explain its impact on modulating host-specific immune response, which needs functional experimental verification. A possible explanation behind that presence could be the more adaptive nature of the virus towards reverse transmission by being less virulent, i.e., from human to other animals, as observed in recent reports[80,81].

3.4 N Protein Mutation: Augmenting Nucleocapsid Stability and Exerting Miscellaneous Effects

Our study has observed that the combined mutation (N: p.RG203-204KR) causes no conformational change in secondary and 3D structures (Figure S1 and Figure 7, respectively) of the conserved SR-rich site (184 → 204) in the linker region (LKR: 183 → 254) of the N protein (supplementary Figure S7), but there is a minor alteration among buried or exposed residues (supplementary Figure S1c and Figure 8b). The superimposed 3D structures showed structural deviation, rather at ^{231}ESKMSGKGQQQQGQTVT^{247} of the LKR (Figure 7), corresponding to the high destabilization of the mutated ($KR_{203\text{-}204}$) protein (Table 2).

Impedance to form particular SR-motif due to RG→KR mutation might disrupt the phosphorylation catalyzed by host glycogen synthase kinase-3[82]. After virus enters into the cell, this synchronized hypo-phosphorylation of $KR_{203\text{-}204}$ protein should make the viral ribonucleoprotein (RNP) unwind in a slower but more organized fashion that might have an impact upon translation and immune-modulation[83-85]. In $KR_{203\text{-}204}$, replacement of glycine

with arginine may increase the nucleocapsid (N protein-RNA complex) stability by forming stronger electrostatic and ionic interactions due to increased positive charge[86,87]. Besides, the more disordered orientation of the downstream LKR site[83] and highly destabilizing property of $KR_{203\text{-}204}$ may assist in the packaging of a stable RNP[88,89]. N protein also utilizes the dynamic nature of the intrinsically disordered linker region (LKR) that controls its affinity towards M protein, self-monomer, 5'UTR, and cellular proteins[90-92]. The phosphorylation at the LKR site may play an essential role to regulate these interactions[86]. These plausible interactions and impact upon mutations are depicted in Figure 1.

3.5 Silent Mutations may not be Silent

The C241T of 5'UTR (untranslated region), a single nucleotide 'silent' mutation, is located at the UUCGU pentaloop part of the stem-loop region (SLR5B). This pentaloop of 5'UTR remains unchanged and maintains a particular structure with a potential role in viral packaging[91,93]. The RNA secondary structural analysis in our study predicted that there is no change in the 241T structure (supplementary Figure S8a). However, C241T is present just upstream to the ORF1a start codon (266-268 position) and may be involved in differential RNA binding affinity to the ribosome and translational factors[94].

In the case of multi-domain NSP3 (papain-like protease), we have observed superior stability of the RNA after gaining the synonymous mutation 3037C<T (C318T) where wild and mutant RNA structure has -151.63 and -153.03 Kcal/mol, respectively (Supplementary Figure S7b-c). A more stable secondary structure of (+)-ssRNA as observed in the mutated NSP3 protein coding sequence corresponds to the slower translational elongation that generally contributes to a range of abnormalities resulting in low translation efficiency affecting posttranslational modifications as a part of protein regulation[95]. This silent mutation is located within the flexible loop of the NSP3 ubiquitin-like domain 1 (Ubl1). In SARS-CoV, Ubl1 was reported to bind with single-stranded RNA containing AUA patterns and interact with the nucleocapsid (N) protein[96,97]. Besides, Ubl1 was likely to bind with several signature repeats in 5′-UTR in SARS-CoV-2 genome[98]. Finally, change in T445C in leader protein may not cause any change in expression or others since the structure (data not shown) and energy are same -172.34 kcal/mol. Figure 1 represents the overall possible scenario due to these silent mutations.

3.6 Epistatic Effects of the Co-occurring Mutations on Viral Replication and Transmission: A Plausible Hypothesis

The co-occurring mutations, as defined by the presence of simultaneous multi-site variations in the same or different proteins or in the genome, have provided new insights into the dynamic epistatic network by employing differential molecular interactions. The epistatic effects of the mutations were reported to control viral fitness and virulence through modulating replication cycle and virus-host interactions, as observed before for Influenza and Ebola virus[99-104]. For instance, the detrimental effect of R384G on influenza A fitness was overcome by the co-occurring mutation E375G[100,103], and co-occurring mutations at the antigenic sites of influenza hemagglutinin can also drive viral evolution[102,104]. The correlation of the co-occurring GP-L mutations affect Ebola virus virulence and thus case fatality rate[101]. The co-occurring mutations of the major SARS-CoV-2 clades discussed in this work showed epistatic link[22,23], and positive selection pressure except for the synonymous mutations[22,24,25] that were also shown in Observable site (https://observablehq.com/). We propose here a hypothesis (model) on how the co-occurring mutations of SARS-CoV-2 might influence replication and transmission fitness of the major clade strains.

Between two important G clade-featured co-occurring mutations, the p:D614G of the S protein and p:P323L of RdRp, we speculated no interlinked functional relationship (Figure 1) and the sequence based prediction showed no potentially significant epistatic link as well[23]. These seemingly unrelated mutations can cumulatively escalate the infectiousness of the virus as a result of higher viral load and shorter burst time. The S:p.D614G might assist in rapid entry into the host cells with an efficient elastase-2 activity and higher transmissibility and/or aggressiveness of G_{614} mutant[19,20] and could be related to elastase-2 or human neutrophil elastase (hNE) concentration during inflammation[105]. Besides, higher levels of functional S protein observed in G614 strains can increase the chance of host-to-host transmission[59]. The RdRp:p:P323L may rather boost up the replication by a faster RNA processing (exiting) that can open up the avenue to generate strains with significantly ($p<0.0001$) higher number of mutations. This increased mutation rate in L_{323} mutants can surpass the constant proof-reading fidelity[106] and evolve into a greater number of variants within a population (Figure 1), that might help adapt more quickly in adverse climatic condition, evade the immune response, and survive within different selective pressure[107,108].

NSP3 is a scaffolding protein for the replication-transcription complex, and the possible change in its structure may affect the overall dynamics of viral replication[96,97]. P323L mutation of RdRp may change binding affinity to the Ubl1 region of NSP3[109] (Figure 1). Significant epistatic links of NSP3:C3037T with spike and RdRp mutations was also

411 reported by Zeng et al. (2020)[23]. In contrast, we could not predict any possible association of
412 the 5′UTR:C241T mutation with the S, RdRp, and NSP3 mutated proteins as also shown by
413 sequence analysis in Zeng et al. (2020)[23]. The rapid within-host replication and modified
414 replication dynamics might be correlated with the fitness of G clade strains[110].

415 The mutant N protein may have an impact on viral replication and transcription, like
416 other coronaviruses[92], through the binding with NSP3 protein that is linked to RdRp centered
417 replication complex. The N protein can also affect the membrane stability by yet
418 uncharacterized interaction with the M protein, which could ultimately produce more stable
419 virion particles[111-113]. A stronger N protein-RNA complex provokes slower intracellular
420 immune response[84], and at the same time, can still remain highly contagious and aggressive
421 because of the concurrent presence of G clade-featured S protein and RdRp mutations (Figure
422 1). The GR strains could hence attain a plausible advantage over G and GH by a more
423 orchestrated, delicately balanced synergistic effects on replication and transmission fitness.
424 These epistatic effects might have increased the fitness by hiding the virus from cellular
425 immunity of the host and increasing stability in the environment, i.e., more transmissible
426 through air and surface. Conversely, we have not found any literature for even other
427 coronaviruses that correlated the ORF3a: p.Q57H with rest of the co-occurring mutations.
428 The H_{57} mutant, possibly linked to the mild or asymptomatic cases, may allow the silent
429 transmission and increase the chance of viral spread by lowering the activation of
430 inflammatory response (Figure 1), such as reduced viral particle release and cytokine
431 storm[21,114,115].

432 The GV strains featuring an A222V mutation in the S protein along with other
433 mutations of the clade G was reported to have probably no effect on the viral transmission,
434 severity, and escaping antibody due to its structural position, rather superspreading founder
435 events after lifting up of travel restriction in Europe and lack of effective containment might
436 be the cause of its spreading within Europe[17,116]. There was, however, speculation about the
437 effect of this mutation on immunogenicity since computational analysis predicted its location
438 within T-cell target region[117,118]. The A220V mutation in the N protein of the GV clade
439 showed a slightly more stable formation of the mutated N protein linker region (Table 2) with
440 no change in the chemical properties, that might affect RNA binding affinity[88], but how this
441 change might give an advantage for the GV strains is a question for further experiments.
442 However, different mutations at positions 220 in N found in other major lineages showed no
443 clear evidence of phenotypic consequence (Hodcroft et al., 2020). There was also no

epistatically linked pairing between GV clade co-occurring mutations[22,23]. Altogether, the co-occurring mutations of GV strains might not affect transmission fitness.

Vaccine inequity, immunocompromised patients, and a tremendous number of hosts are now frequently introducing variants with mutations in the receptor binding domain (RBD) of spike protein, i.e., lineage B.1.1.7, a variant of concern under GR clade, consists of 17 mutations (14 nonsynonymous and 3 deletions) in spike, N, ORF1ab, and ORF8 proteins, as well as, 6 silent mutations[119,120]. The newly added mutations in this lineage on top of the original GR clade-featured ones in the genome might play most crucial role both in increasing transmission fitness and a slightly reduced neutralization to antibody by showing epistatic effects[121121,122]. Other emerging variants (B.1.617.*, B.1.351, B.1.258, etc.) with additional co-occurring mutations are also the descendants of these major clades. Future studies are necessary to investigate the roles of the 'mutation package' present in each of these variants of concern/interest.

4. CONCLUSION

In 2020, the course of COVID-19 pandemic was dominated by the G, GH, GR, and GV clades. The G clade-featured co-occurring mutations might increase the viral load, alter immune responses in host and modulate intra-host virus genome plasticity that arises the speculation of their probable role in frequent transmission. The GR and GH clade mutant with the signature mutation, respectively, in nucleocapsid and ORF3a protein might contribute to immune response of the host and viral transmission. The GV strains however could have spread quickly by superspreading events with no apparent epistatic effect. Therefore, the fitness of SARS-CoV-2 may increase in terms of replication and transmission where viral strains are always giving their spread capacity within a population the top priority by calibrating the infection cycle. However, further *in vivo* and *ex vivo* studies and more investigations are required to prove and bolster this hypothesis.

Data Availability

All the sequence and structural data were taken from the GISAID (https://www.gisaid.org/) and RCSB PDB (https://www.rcsb.org/) as mentioned in the methodology section. We provide all the necessary information such as accession numbers, date-based data source for helping readers and reviewers to check the authenticity of the work.

Acknowledgments

We would like to acknowledge the team at GISAID for creating SARS-CoV-2 global database. The funding of the research was provided by Jashore University of Science and Technology. We appreciate to the Microbial Genetics and Bioinformatics Laboratory of University of Dhaka for the support of the high-performance computer access. We thanked M. Shaminur Rahman for their technical assistance in protein structure stability analyses.

Conflict of Interest Statement

We have no conflict of interest.

Biographical Note

A. S. M. Rubayet Ul Alam (ASMRUA) is an assistant professor in the Department of Microbiology, Jashore University of Science and Technology. His research mainly focuses on molecular biology, data analysis, and bioinformatics.

Ovinu Kibria Islam (OKI) is an assistant professor in the Department of Microbiology, Jashore University of Science and Technology. His research activity is focused on molecular biology and big data analysis.

Md. Shazid Hasan (MSH) is an assistant professor in the Department of Microbiology, Jashore University of Science and Technology. His research activity is focused on molecular biology and bioinformatics.

Mir Raihanul Islam (MRI) is the Senior Research Associate of BRAC James P Grant School of Public Health, BRAC University who is expert in statistical analysis and epidemiological study and is currently working on many active researches related to public health.

Shafi Mahmud (SM) is working as a Master's thesis student in the department of Genetic Engineering and Biotechnology, University of Rajshahi, Rajshai-6205, Bangladesh.

Hassan M. Al□Emran (HMA) is the Chairman in the Department of Biomedical Engineering, Jashore University of Science and Technology, Jashore-7408, Bangladesh. His research mainly focuses on clinical microbiology and infectious diseases.

Dr. Iqbal Kabir Jahid (IKJ) is a Professor and Chairman in the Department of Microbiology, Jashore University of Science and Technology. His research mainly focuses on molecular biology.

Keith A. Crandall (KAC) is a Professor in the Department of Biostatistics & Bioinformatics and the director of Computational Biology Institute, Director of Genomics Core, Milken Institute School of Public Health, The George Washington University, Washington, DC, USA.

M. Anwar Hossain (MAH) is the director of Genome Center, and Vice Chancellor of Jashore University of Science and Technology. He is an expert in molecular biology, virology and vaccine development.

Authors' Contribution

IKJ, OKI and ASMRUA hypothesized about the work. ASMRUA performed the sequence analysis part after OKI and MSH compiled the dataset. The Python coding, structural (both RNA and protein), and protein docking were done by ASMRUA. MSH predicted protein structure in I-TASSER and performed stability analysis in DynaMut. SM performed the molecular dynamics study. HMA performed the statistical analysis. HMA then reviewed and organized the manuscript expertly. IKJ, KAC and MAH supervised, suggested and revised the write-up to produce the final draft.

REFERENCES

1. Hoffmann M, Kleine-Weber H, Pöhlmann S. A multibasic cleavage site in the spike protein of SARS-CoV-2 is essential for infection of human lung cells. *Molecular Cell.* 2020.
2. Hoque MN, Chaudhury A, Akanda MAM, Hossain MA, Islam MT. Genomic diversity and evolution, diagnosis, prevention, and therapeutics of the pandemic COVID-19 disease. *PeerJ.* 2020;8:e9689.
3. Petersen E, Koopmans M, Go U, et al. Comparing SARS-CoV-2 with SARS-CoV and influenza pandemics. *The Lancet infectious diseases.* 2020.
4. Romano M, Ruggiero A, Squeglia F, Maga G, Berisio R. A Structural View of SARS-CoV-2 RNA Replication Machinery: RNA Synthesis, Proofreading and Final Capping. *Cells.* 2020;9(5):1267.
5. Rahman MS, Hoque MN, Islam MR, et al. Epitope-based chimeric peptide vaccine design against S, M and E proteins of SARS-CoV-2 etiologic agent of global pandemic COVID-19: an in silico approach. *PeerJ.* 2020;8:e9572.
6. Yoshimoto FK. The Proteins of Severe Acute Respiratory Syndrome Coronavirus-2 (SARS CoV-2 or n-COV19), the Cause of COVID-19. *The protein journal.* 2020;39(3):198-216.
7. Callaway E. The coronavirus is mutating-does it matter? *Nature.* 2020;585(7824):174-177.
8. Islam MR, Hoque MN, Rahman MS, et al. Genome-wide analysis of SARS-CoV-2 virus strains circulating worldwide implicates heterogeneity. *Scientific reports.* 2020;10(1):1-9.

9. Rahman MS, Islam MR, Hoque MN, et al. Comprehensive annotations of the mutational spectra of SARS□CoV□2 spike protein: a fast and accurate pipeline. *Transboundary and emerging diseases*. 2020.
10. Eskier D, Karakülah G, Suner A, Oktay Y. RdRp mutations are associated with SARS-CoV-2 genome evolution. *PeerJ*. 2020;8(e):9587.
11. Hassan SS, Choudhury PP, Basu P, Jana SS. Molecular conservation and Differential mutation on ORF3a gene in Indian SARS-CoV2 genomes. *Genomics*. 2020.
12. Shaminur Rahman M, Rafiul Islam M, Rubayet Ul Alam A, et al. Evolutionary dynamics of SARS□CoV□2 nucleocapsid (N) protein and its consequences. *Journal of medical virology*.
13. Hamed SM, Elkhatib WF, Khairalla AS, Noreddin AM. Global dynamics of SARS-CoV-2 clades and their relation to COVID-19 epidemiology. *Scientific reports*. 2021;11(1):1-8.
14. Yin C. Genotyping coronavirus SARS-CoV-2: methods and implications. *Genomics*. 2020;112(5):3588-3596.
15. Mercatelli D, Giorgi FM. Geographic and genomic distribution of SARS-CoV-2 mutations. *Frontiers in microbiology*. 2020;11:1800.
16. Rambaut A, Holmes EC, O'Toole Á, et al. A dynamic nomenclature proposal for SARS-CoV-2 lineages to assist genomic epidemiology. *Nature microbiology*. 2020;5(11):1403-1407.
17. Hodcroft EB, Zuber M, Nadeau S, et al. Emergence and spread of a SARS-CoV-2 variant through Europe in the summer of 2020. *medRxiv*. 2020.
18. Grubaugh ND, Hanage WP, Rasmussen AL. Making sense of mutation: what D614G means for the COVID-19 pandemic remains unclear. *Cell*. 2020.
19. Plante JA, Liu Y, Liu J, et al. Spike mutation D614G alters SARS-CoV-2 fitness. *Nature*. 2020:1-9.
20. Hou YJ, Chiba S, Halfmann P, et al. SARS-CoV-2 D614G variant exhibits efficient replication ex vivo and transmission in vivo. *Science*. 2020.
21. Issa E, Merhi G, Panossian B, Salloum T, Tokajian S. SARS-CoV-2 and ORF3a: Nonsynonymous Mutations, Functional Domains, and Viral Pathogenesis. *Msystems*. 2020;5(3).
22. Rochman ND, Wolf YI, Faure G, Mutz P, Zhang F, Koonin EV. Ongoing global and regional adaptive evolution of sars-cov-2. *Proceedings of the National Academy of Sciences*. 2021;118(29).
23. Zeng H-L, Dichio V, Horta ER, Thorell K, Aurell E. Global analysis of more than 50,000 SARS-CoV-2 genomes reveals epistasis between eight viral genes. *Proceedings of the National Academy of Sciences*. 2020;117(49):31519-31526.
24. Presti AL, Rezza G, Stefanelli P. Selective pressure on SARS-CoV-2 protein coding genes and glycosylation site prediction. *Heliyon*. 2020;6(9):e05001.
25. Berrio A, Gartner V, Wray GA. Positive selection within the genomes of SARS-CoV-2 and other Coronaviruses independent of impact on protein function. *PeerJ*. 2020;8:e10234.
26. Rodrigues CH, Pires DE, Ascher DB. DynaMut: predicting the impact of mutations on protein conformation, flexibility and stability. *Nucleic acids research*. 2018;46(W1):W350-W355.
27. Schymkowitz J, Borg J, Stricher F, Nys R, Rousseau F, Serrano L. The FoldX web server: an online force field. *Nucleic acids research*. 2005;33(suppl_2):W382-W388.
28. Delgado J, Radusky LG, Cianferoni D, Serrano L. FoldX 5.0: working with RNA, small molecules and a new graphical interface. *Bioinformatics*. 2019;35(20):4168-4169.

29. Rost B, Yachdav G, Liu J. The predictprotein server. *Nucleic acids research.* 2004;32(suppl_2):W321-W326.
30. Waterhouse A, Bertoni M, Bienert S, et al. SWISS-MODEL: homology modelling of protein structures and complexes. *Nucleic acids research.* 2018;46(W1):W296-W303.
31. Webb B, Sali A. Comparative protein structure modeling using MODELLER. *Current protocols in bioinformatics.* 2016;54(1):5.6. 1-5.6. 37.
32. Roy A, Kucukural A, Zhang Y. I-TASSER: a unified platform for automated protein structure and function prediction. *Nature protocols.* 2010;5(4):725-738.
33. Wang Q, Wu J, Wang H, et al. Structural basis for RNA replication by the SARS-CoV-2 polymerase. *Cell.* 2020;182(2):417-428. e413.
34. Van Zundert G, Rodrigues J, Trellet M, et al. The HADDOCK2. 2 web server: user-friendly integrative modeling of biomolecular complexes. *Journal of molecular biology.* 2016;428(4):720-725.
35. Xue LC, Rodrigues JP, Kastritis PL, Bonvin AM, Vangone A. PRODIGY: a web server for predicting the binding affinity of protein–protein complexes. *Bioinformatics.* 2016;32(23):3676-3678.
36. Hu J, He CL, Gao Q, et al. The D614G mutation of SARS-CoV-2 spike protein enhances viral infectivity. *bioRxiv.* 2020.
37. de Vries SJ, Bonvin AM. CPORT: a consensus interface predictor and its performance in prediction-driven docking with HADDOCK. *PloS one.* 2011;6(3):e17695.
38. Yan Y, Tao H, He J, Huang S-Y. The HDOCK server for integrated protein–protein docking. *Nature protocols.* 2020;15(5):1829-1852.
39. Krieger E, Nielsen JE, Spronk CA, Vriend G. Fast empirical pKa prediction by Ewald summation. *Journal of molecular graphics and modelling.* 2006;25(4):481-486.
40. Krieger E, Vriend G. New ways to boost molecular dynamics simulations. *Journal of computational chemistry.* 2015;36(13):996-1007.
41. Chowdhury KH, Chowdhury M, Mahmud S, et al. Drug Repurposing Approach against Novel Coronavirus Disease (COVID-19) through Virtual Screening Targeting SARS-CoV-2 Main Protease. *Biology.* 2021;10(1):2.
42. Pramanik SK, Mahmud S, Paul GK, et al. Fermentation optimization of cellulase production from sugarcane bagasse by Bacillus pseudomycoides and molecular modeling study of cellulase. *Current Research in Microbial Sciences.* 2021;2:100013.
43. Swargiary A, Mahmud S, Saleh MA. Screening of phytochemicals as potent inhibitor of 3-chymotrypsin and papain-like proteases of SARS-CoV2: an in silico approach to combat COVID-19. *Journal of Biomolecular Structure and Dynamics.* 2020:1-15.
44. Yan H, Yu C. Repair of full-thickness cartilage defects with cells of different origin in a rabbit model. *Arthroscopy: The Journal of Arthroscopic & Related Surgery.* 2007;23(2):178-187.
45. Zuker M. Mfold web server for nucleic acid folding and hybridization prediction. *Nucleic acids research.* 2003;31(13):3406-3415.
46. Huston NC, Wan H, Tavares RdCA, Wilen C, Pyle AM. Comprehensive in-vivo secondary structure of the SARS-CoV-2 genome reveals novel regulatory motifs and mechanisms. *BioRxiv.* 2020.
47. Rane JS, Chatterjee A, Kumar A, Ray S. Targeting SARS-CoV-2 Spike Protein of COVID-19 with Naturally Occurring Phytochemicals: An in Silco Study for Drug Development. In: ChemRxiv; 2020.
48. Souza PF, Lopes FE, Amaral JL, Freitas CD, Oliveira JT. A molecular docking study revealed that synthetic peptides induced conformational changes in the structure of

SARS-CoV-2 spike glycoprotein, disrupting the interaction with human ACE2 receptor. *International journal of biological macromolecules.* 2020;164:66-76.

49. Elfiky AA. Ribavirin, Remdesivir, Sofosbuvir, Galidesivir, and Tenofovir against SARS-CoV-2 RNA dependent RNA polymerase (RdRp): A molecular docking study. *Life sciences.* 2020:117592.
50. Aftab SO, Ghouri MZ, Masood MU, et al. Analysis of SARS-CoV-2 RNA-dependent RNA polymerase as a potential therapeutic drug target using a computational approach. *Journal of translational medicine.* 2020;18(1):1-15.
51. Phan T. Genetic diversity and evolution of SARS-CoV-2. *Infection, genetics and evolution.* 2020;81:104260.
52. Belouzard S, Chu VC, Whittaker GR. Activation of the SARS coronavirus spike protein via sequential proteolytic cleavage at two distinct sites. *Proceedings of the National Academy of Sciences.* 2009;106(14):5871-5876.
53. Korber B, Fischer W, Gnanakaran S, et al. Tracking changes in SARS-CoV-2 Spike: evidence that D614G increases infectivity of the COVID-19 virus. *Cell.* 2020.
54. Bhattacharyya C, Das C, Ghosh A, et al. SARS-CoV-2 mutation 614G creates an elastase cleavage site enhancing its spread in high AAT-deficient regions. *Infection, Genetics and Evolution.* 2021:104760.
55. Perona JJ, Craik CS. Structural basis of substrate specificity in the serine proteases. *Protein Science.* 1995;4(3):337-360.
56. Fu Z, Thorpe M, Akula S, Chahal G, Hellman LT. Extended cleavage specificity of human neutrophil elastase, human proteinase 3, and their distant ortholog clawed frog PR3—three elastases with similar primary but different extended specificities and stability. *Frontiers in Immunology.* 2018;9:2387.
57. Li F. Structure, function, and evolution of coronavirus spike proteins. *Annual review of virology.* 2016;3:237-261.
58. Walls AC, Tortorici MA, Snijder J, et al. Tectonic conformational changes of a coronavirus spike glycoprotein promote membrane fusion. *Proceedings of the National Academy of Sciences.* 2017;114(42):11157-11162.
59. Zhang L, Jackson CB, Mou H, et al. SARS-CoV-2 spike-protein D614G mutation increases virion spike density and infectivity. *Nature communications.* 2020;11(1):1-9.
60. Weissman D, Alameh M-G, de Silva T, et al. D614G spike mutation increases SARS CoV-2 susceptibility to neutralization. *Cell host & microbe.* 2021;29(1):23-31. e24.
61. Wrapp D, Wang N, Corbett KS, et al. Cryo-EM structure of the 2019-nCoV spike in the prefusion conformation. *Science.* 2020;367(6483):1260-1263.
62. Hillen HS, Kokic G, Farnung L, Dienemann C, Tegunov D, Cramer P. Structure of replicating SARS-CoV-2 polymerase. *Nature.* 2020:1-6.
63. Yin W, Mao C, Luan X, et al. Structural basis for inhibition of the RNA-dependent RNA polymerase from SARS-CoV-2 by remdesivir. *Science.* 2020.
64. Kirchdoerfer RN, Ward AB. Structure of the SARS-CoV nsp12 polymerase bound to nsp7 and nsp8 co-factors. *Nature communications.* 2019;10(1):1-9.
65. Gao Y, Yan L, Huang Y, et al. Structure of the RNA-dependent RNA polymerase from COVID-19 virus. *Science.* 2020;368(6492):779-782.
66. Chand GB, Banerjee A, Azad GK. Identification of novel mutations in RNA-dependent RNA polymerases of SARS-CoV-2 and their implications on its protein structure. *bioRxiv.* 2020.
67. Eskier D, Karakülah G, Suner A, Oktay Y. RdRp mutations are associated with SARS-CoV-2 genome evolution. *bioRxiv.* 2020.

68. Kern DM, Sorum B, Hoel CM, et al. Cryo-EM structure of the SARS-CoV-2 3a ion channel in lipid nanodiscs. *BioRxiv*. 2020.
69. Malasics A, Gillespie D, Nonner W, Henderson D, Eisenberg B, Boda D. Protein structure and ionic selectivity in calcium channels: Selectivity filter size, not shape, matters. *Biochimica et Biophysica Acta (BBA)-Biomembranes.* 2009;1788(12):2471-2480.
70. Naranjo D, Moldenhauer H, Pincuntureo M, Díaz-Franulic I. Pore size matters for potassium channel conductance. *Journal of General Physiology.* 2016;148(4):277-291.
71. Stephens RF, Guan W, Zhorov BS, Spafford JD. Selectivity filters and cysteine-rich extracellular loops in voltage-gated sodium, calcium, and NALCN channels. *Frontiers in Physiology.* 2015;6:153.
72. Suárez-Delgado E, Islas LD. Ion Channels: A novel origin for calcium selectivity. *Elife.* 2020;9:e55216.
73. Kondratskyi A, Kondratska K, Skryma R, Prevarskaya N. Ion channels in the regulation of apoptosis. *Biochimica et Biophysica Acta (BBA)-Biomembranes.* 2015;1848(10):2532-2546.
74. Yue Y, Nabar NR, Shi C-S, et al. SARS-Coronavirus Open Reading Frame-3a drives multimodal necrotic cell death. *Cell death & disease.* 2018;9(9):1-15.
75. Pinton P, Giorgi C, Siviero R, Zecchini E. Rizzuto R. *Bcl-2 and Ca.* 2006;2:1409-1418.
76. Nieva JL, Madan V, Carrasco L. Viroporins: structure and biological functions. *Nature Reviews Microbiology.* 2012;10(8):563-574.
77. Ren Y, Shu T, Wu D, et al. The ORF3a protein of SARS-CoV-2 induces apoptosis in cells. *Cellular & molecular immunology.* 2020:1-3.
78. Castaño-Rodriguez C, Honrubia JM, Gutiérrez-Álvarez J, et al. Role of severe acute respiratory syndrome coronavirus viroporins E, 3a, and 8a in replication and pathogenesis. *MBio.* 2018;9(3).
79. Boni MF, Lemey P. Evolutionary origins of the SARS-CoV-2 sarbecovirus lineage responsible for the COVID-19 pandemic. *Nature microbiology.* 2020.
80. Halfmann PJ, Hatta M, Chiba S, et al. Transmission of SARS-CoV-2 in domestic cats. *New England Journal of Medicine.* 2020.
81. Shi J, Wen Z, Zhong G, et al. Susceptibility of ferrets, cats, dogs, and other domesticated animals to SARS–coronavirus 2. *Science.* 2020;368(6494):1016-1020.
82. Tylor S, Andonov A, Cutts T, et al. The SR-rich motif in SARS-CoV nucleocapsid protein is important for virus replication. *Canadian journal of microbiology.* 2009;55(3):254-260.
83. Järvelin AI, Noerenberg M, Davis I, Castello A. The new (dis) order in RNA regulation. *Cell Communication and Signaling.* 2016;14(1):9.
84. Kikkert M. Innate immune evasion by human respiratory RNA viruses. *Journal of innate immunity.* 2020;12(1):4-20.
85. Kopecky-Bromberg SA, Martínez-Sobrido L, Frieman M, Baric RA, Palese P. Severe acute respiratory syndrome coronavirus open reading frame (ORF) 3b, ORF 6, and nucleocapsid proteins function as interferon antagonists. *Journal of virology.* 2007;81(2):548-557.
86. McBride R, Van Zyl M, Fielding BC. The coronavirus nucleocapsid is a multifunctional protein. *Viruses.* 2014;6(8):2991-3018.
87. Sokalingam S, Raghunathan G, Soundrarajan N, Lee S-G. A study on the effect of surface lysine to arginine mutagenesis on protein stability and structure using green fluorescent protein. *PloS one.* 2012;7(7):e40410.

88. Chang C-k, Hou M-H, Chang C-F, Hsiao C-D, Huang T-h. The SARS coronavirus nucleocapsid protein–forms and functions. *Antiviral research.* 2014;103:39-50.
89. Haynes C, Iakoucheva LM. Serine/arginine-rich splicing factors belong to a class of intrinsically disordered proteins. *Nucleic acids research.* 2006;34(1):305-312.
90. Carlson CR, Asfaha, J. B., Ghent, C. M., Howard, C. J, Hartooni, N., Safari, M, ... & Morgan, D. O. Phosphoregulation of Phase Separation by the SARS-CoV-2 N Protein Suggests a Biophysical Basis for its Dual Functions. *Molecular Cell.* 2020;11:025.
91. Schuster NA. Using the nucleocapsid protein to investigate the relationship between SARS-CoV-2 and closely related bat and pangolin coronaviruses. *BioRxiv.* 2020.
92. de Haan CA, Rottier PJ. Molecular interactions in the assembly of coronaviruses. *Advances in virus research.* 2005;64:165-230.
93. Huston NC, Wan H, Strine MS, Tavares RdCA, Wilen CB, Pyle AM. Comprehensive in vivo secondary structure of the SARS-CoV-2 genome reveals novel regulatory motifs and mechanisms. *Molecular cell.* 2021;81(3):584-598. e585.
94. Kristofich J, Morgenthaler AB, Kinney WR, et al. Synonymous mutations make dramatic contributions to fitness when growth is limited by a weak-link enzyme. *PLoS genetics.* 2018;14(8):e1007615.
95. Mitra S, Ray SK, Banerjee R. Synonymous codons influencing gene expression in organisms. *Research and Reports in Biochemistry.* 2016;6:57.
96. Hurst KR, Ye R, Goebel SJ, Jayaraman P, Masters PS. An interaction between the nucleocapsid protein and a component of the replicase-transcriptase complex is crucial for the infectivity of coronavirus genomic RNA. *Journal of virology.* 2010;84(19):10276-10288.
97. Hurst KR, Koetzner CA, Masters PS. Characterization of a critical interaction between the coronavirus nucleocapsid protein and nonstructural protein 3 of the viral replicase-transcriptase complex. *Journal of virology.* 2013;87(16):9159-9172.
98. Serrano P, Johnson MA, Almeida MS, et al. Nuclear magnetic resonance structure of the N-terminal domain of nonstructural protein 3 from the severe acute respiratory syndrome coronavirus. *Journal of virology.* 2007;81(21):12049-12060.
99. Du X, Wang Z, Wu A, et al. Networks of genomic co-occurrence capture characteristics of human influenza A (H3N2) evolution. *Genome research.* 2008;18(1):178-187.
100. Rimmelzwaan G, Berkhoff E, Nieuwkoop N, Smith DJ, Fouchier R, Osterhaus A. Full restoration of viral fitness by multiple compensatory co-mutations in the nucleoprotein of influenza A virus cytotoxic T-lymphocyte escape mutants. *Journal of general virology.* 2005;86(6):1801-1805.
101. Deng L, Liu M, Hua S, et al. Network of co-mutations in Ebola virus genome predicts the disease lethality. *Cell research.* 2015;25(6):753-756.
102. Chen H, Zhou X, Zheng J, Kwoh C-K. Rules of co-occurring mutations characterize the antigenic evolution of human influenza A/H3N2, A/H1N1 and B viruses. *BMC medical genomics.* 2016;9(3):69.
103. Rimmelzwaan GF, Kreijtz JH, Bodewes R, Fouchier RA, Osterhaus AD. Influenza virus CTL epitopes, remarkably conserved and remarkably variable. *Vaccine.* 2009;27(45):6363-6365.
104. Lyons DM, Lauring AS. Mutation and epistasis in influenza virus evolution. *Viruses.* 2018;10(8):407.
105. Mohamed MM, El-Shimy IA, Hadi MA. Neutrophil Elastase Inhibitors: A potential prophylactic treatment option for SARS-CoV-2-induced respiratory complications? In: BioMed Central; 2020.

106. Smith EC, Sexton NR, Denison MR. Thinking outside the triangle: replication fidelity of the largest RNA viruses. *Annual Review of Virology.* 2014;1:111-132.
107. Pfeiffer JK, Kirkegaard K. Increased fidelity reduces poliovirus fitness and virulence under selective pressure in mice. *PLoS Pathog.* 2005;1(2):e11.
108. Vignuzzi M, Stone JK, Arnold JJ, Cameron CE, Andino R. Quasispecies diversity determines pathogenesis through cooperative interactions in a viral population. *Nature.* 2006;439(7074):344-348.
109. Lei J, Kusov Y, Hilgenfeld R. Nsp3 of coronaviruses: Structures and functions of a large multi-domain protein. *Antiviral research.* 2018;149:58-74.
110. Skjesol A, Skjæveland I, Elnæs M, et al. IPNV with high and low virulence: host immune responses and viral mutations during infection. *Virology journal.* 2011;8(1):1-14.
111. Schoeman D, Fielding BC. Coronavirus envelope protein: current knowledge. *Virology journal.* 2019;16(1):1-22.
112. Escors D, Ortego J, Laude H, Enjuanes L. The membrane M protein carboxy terminus binds to transmissible gastroenteritis coronavirus core and contributes to core stability. *Journal of virology.* 2001;75(3):1312-1324.
113. J Alsaadi EA, Jones IM. Membrane binding proteins of coronaviruses. *Future Virology.* 2019;14(4):275-286.
114. Bai Y, Yao L, Wei T, et al. Presumed asymptomatic carrier transmission of COVID-19. *Jama.* 2020;323(14):1406-1407.
115. Quan-Xin L, Xiao-Jun T, Qiu-Lin S, et al. Clinical and immunological assessment of asymptomatic SARS-CoV-2 infections. *Nature medicine.* 2020.
116. McCallum M, De Marco A, Lempp F, et al. N-terminal domain antigenic mapping reveals a site of vulnerability for SARS-CoV-2. *bioRxiv.* 2021.
117. Zhang B-z, Hu Y-f, Chen L-l, et al. Mining of epitopes on spike protein of SARS-CoV-2 from COVID-19 patients. *Cell research.* 2020;30(8):702-704.
118. Mateus J, Grifoni A, Tarke A, et al. Selective and cross-reactive SARS-CoV-2 T cell epitopes in unexposed humans. *Science.* 2020;370(6512):89-94.
119. Volz E, Mishra S, Chand M, et al. Transmission of SARS-CoV-2 Lineage B. 1.1. 7 in England: Insights from linking epidemiological and genetic data. *medRxiv.* 2021:2020.2012. 2030.20249034.
120. Muik A, Wallisch A-K, Sänger B, et al. Neutralization of SARS-CoV-2 lineage B. 1.1. 7 pseudovirus by BNT162b2 vaccine–elicited human sera. *Science.* 2021.
121. McCarthy KR, Rennick LJ, Nambulli S, et al. Recurrent deletions in the SARS-CoV-2 spike glycoprotein drive antibody escape. *Science.* 2021.
122. Kemp S, Collier D, Datir R, et al. Neutralising antibodies drive Spike mediated SARS-CoV-2 evasion (medRxiv). *bioRxiv.* 2020.

Table 1. The scores of HADDOCK, PRODIGY (ΔG and Kd (M) at 37.0 □) for RdRp/NSP8 and Spike-Elastase docked complex.

Variables	types	RdRp/NSP8	Spike-Elastase
HADDOCK score	Wild	-82.2 +/- 7.8	-43.0 +/- 8.9
	Mutant	-118.3 +/- 2.5	-61.9 +/- 4.5
ΔG (kcal mol^{-1})	Wild	-10.6	-13.3
	Mutant	-10.5	-13.7
Kd (M) at 37.0 □	Wild	3.5E^{-08}	4.5E^{-10}

	Mutant	$3.9E^{-08}$	$2.3E^{-10}$
Number of interfacial contacts (ICs) per property	Wild	charged-charged (5); charged-polar (9); charged-apolar (15); polar-polar (2); polar-apolar (16); and apolar-apolar (21)	charged-charged (17);charged-polar (22);charged-apolar (32);polar-polar (5);polar-apolar (31); and apolar-apolar (23)
	Mutant	charged-charged(5);charged-polar (16);charged-apolar (19); polar-polar (3);polar-apolar(15); apolar-apolar (23)	charged-charged (13);charged-polar (18);charged-apolar (27);polar-polar (4); polar-apolar (28) and apolar-apolar (36)
Associated amino acids of Elastase-2 with possible docking interactions (for spike) or NSP8 (for RdRp)	Wild	P323: Asp(112), Cys(114), Val(115) and Pro (116)	605 (Ser) and 607 (Gln): 36 (Arg); 618 (Thr): 199 (Phe); 619 (Glu): 199 (Phe), Cys (227); 620 (Val): 198 (Cys), 225:227(Gly, Gly, Cys)
	Mutant	P323: Asp(112), Cys(114), Val(115) and Pro (116)	614 (Gly): 101 (Val); 618 (Thr): 181 (Arg), 223-226(Val, Arg, Gly, Gly); 619 (Glu): 103 (Leu), 181(Arg), 222-225(Phe, Val, Arg, Gly), 236 (Ala); 620 (Val): 223-227 (Val, Arg, Gly, Gly, Cys)

Table 2. Assess the effect of mutations on structural dynamics of NSP-12/ RDRP, Spike, NS3 and N Protein of SARS CoV-2 using DynaMut. The value of ΔΔG <0 indicates that the mutation causes destabilization and ΔΔG > 0 represents protein stabilization. For ΔΔSVibENCoM, positive and negative value denotes the increase and decrease of molecular flexibility, respectively.

Protein Name	**Mutation with position**	**ΔΔG DynaMut kcal/mol**	**ΔΔG ENCoM kcal/mol**	**ΔΔG mCSM kcal/mol**	**ΔΔG SDM kcal/mol**	**ΔΔG DUET kcal/mol**	**ΔΔG FoldX (kcal/mol)**	**Results***	**$\Delta\Delta S_{Vib}$ ENCoM kcal.mol^{-1}.K^{-1}**
RdRp	P323L	1.054	-0.441	-0.264	0.700	0.118	-0.733	Stabilizing	-0.551
Spike	D614G	-0.769	+0.408	-0.492	2.530	0.195	+0.289	Destabilizing	0.510
ORF3a	Q57H	0.275	-0.128	0.788	0.520	-0.464	-1.438	Stabilizing	-0.160
N Protein	RG203-04KR	-	-	-	-	-	-3.42262	Highly Destabilizing	-
N protein	A220V	0.109	0.458	-0.586	-1.460	-0.567	+1.6	Stabilizing	-0.572

*The final result of the stability for each protein was determined based on the intra-molecular interactome analysis

Figure 1. Schematic diagram of SARS-CoV-2 replication in cell showcasing the related to S, N, ORF3a, RdRp, NSP3 and 5'-UTR based epistatic interactions.

The replication cycle starts with the ACE2 receptor binding of the spike glycoprotein (S) as cornered at the top-left and finishes with the exocytosis at the top-right. The viruses which do not carry G-, GH- and/or GR-featured mutations in the S, N, ORF3a, RdRp, NSP3 and 5'-UTR are denoted as the wild type where mutants contain those. Throughout the diagram, the red and green color icons such as proteins, genome, and virion represent the wild and mutant type, respectively. For a generalized virion, we used the blue color. Although this theme is not show the co-infection of both types, which might occur in rare occasions, we showed the comparative epistatic effects side-by-side fashion during the whole replication cycle that will make it easy to grasp. Related figure(s) for each protein are shown in the enclosed box. To mean the uncertainty or unknown effects of any mutant proteins/RNA structure, we used the 'question' mark in a pathway and on explanatory box. RdRp- RNA dependent RNA polymerase; NSP14-proof-reading enzyme of SARS-CoV-2; ER- endoplasmic reticulum; ERGIC- endoplasmic

Figure 2. Different structural and stability comparison of wild and mutant spike protein. Structural superposition of wild and mutant spike proteins **(a-b)**; conformation in the S1-S2 **(c)** and S2'sites **(d-e)**; representation of vibrational entropy energy change on the mutant type structure **(f)**; and interatomic interaction prediction of both wild **(g)** and mutant **(h)** types. For Figure a-e, the gray and yellow color represent the wild and mutant protein, respectively. **(a)** The downstream (617-636) of D614G in wild (green) and mutant (red) S protein was focused. Overlapping of the wild (D_{614}) and mutant (G_{614}) S protein showed conformational change in the 3D structures. **(b)** However, the conformational change are in the loop region (618-632) of the proteins thus may potentially play role in interacting with other proteins or enzymes, such as elastase-2 as we focused in this work. **(c)** No change was found in the S1-S2 cleavage site (685-686), depicted in blue color, of the wild and mutant protein. **(d)** Surface and **(e)** cartoon (2°) structure of the superimposed wild and mutant proteins where the S2' (pink) is situated in surface region and do not show any change in

accessibility in the residual loop region. **(f)** The mutant (G_{614}) protein showed higher flexibility in the G^{614} (sticks) and its surroundings (red). The intra-molecular interaction determined the overall stability of the **(g)** wild and **(h)** mutant structure where C_β of D^{614} (aspartic acid at 614; green stick modelled) had two hydrophobic interaction with the benzene rings. This intramolecular contacts stabilize the S protein of wild type and missing of this bond destabilize the mutant (G_{614}) protein. The mutant protein has glycine at 614 which has less chance of interacting with other neighboring amino acids due to its shorter and nonpolar R-group. The color code representing the bond type is presented in each **(g)** and **(h)**.

Figure 3. The molecular docking of wild and mutant with elastase-2. Both the (upper figure) wild (D_{614}) and (lower figure) mutant (G_{614}) version of S protein was shown in golden color whereas the elastase-2 docked to D_{614} and G_{614} in blue and green color, respectively. The enlarged views of the docked site were shown in separate boxes. **(a)** The possible docked residues (stick model) on the wild S protein (warm pink) and elastase-2 (green) are 618(Thr)-619(Glu)-620(Val) and 198(Cys)-199(Phe)-225:227 (Gly, Gly, Cys), respectively. The aspartic acid at 614 is 17.3°A far away from the valine (101), apparently the nearest amino acid of elastase-2 to the cleavage site (615-616). **(b)** The possible interacting residues (stick model) on the mutant S protein (blue) and elastase-2 (warm pink) are 614(Gly)-618(Thr)-619(Glu)-620(Val) and 101(Val)-103(Leu)-181(Arg)-222:227(Phe, Val, Arg, Gly, Gly, Cys), and 236 (Ala) respectively. In this case, the glycine at 614 is only 5.4°A far away from the valine (101), the nearest amino acid of elastase-2 to the cleavage site (615-616).

Figure 4. (a) Both the wild and mutated spike protein had lower RMSD profile till 60ns, then it rised and maintained steady state. Although the spike protein had higher degree of deviation in RMSD profile than RdRp but they did not exceed 3.0Å. The RMSD from demonstrated that mutant and wild RdRp protein complex has initial rise of RMSD profile due to flexibility. Therefore, both RdRp complexes stabilized after 30ns and maintained steady peak. The wild type RdRp complex had little bit higher RMSD peak than mutant RdRp which indicates the more flexible nature of the wild type. (b) The spike protein complex had similar SASA profile and did not change its surface volume and maintained similar trend during the whole simulation time. The higher deviation of SASA indicates that mutant and wild type RdRp had straight line but mutant structure had higher SASA profile which indicates the protein complex had enlarged its surface area. Therefore, mutation in

RdRp protein leads to more expansion of the surface area than wild types as their average SASA value had significant difference. (c) Mutated spike exhibits little more Rg profile than the wild type which correlates with the comparative labile nature of the mutant. The higher level of Rg value defines the loose packaging system and mobile nature of the protein systems. The mutant RdRp had lower level of fluctuations and maintains its integrity in whole simulation time. The wild type RdRp complexes had higher deviations and more mobility than the mutant complex. (d) Any aberration in hydrogen bond number can lead to a higher flexibility. Therefore, the mutant and wild spike protein exhibit same flexibility in terms of H-bonding. The mutant RdRp protein had more hydrogen bonding than the wild types, but they did not differentiate too much and relatively straight line was observed for the protein.

Figure 5. The molecular interaction of mutant RdRp with NSP8. The mutant (L_{323}) RdRp (pale green) and NSP8 (light blue) are interacting as shown in center of the lower figure and an enlarged view of the docked site is presented above within a box. The leucine at 323 interacted with the Asp (112), Cys (114), Val (115), and Pro (116). The wild (P_{323}) RdRp has identical docking interactions with NSP8 (table 4), thus is not presented as separate figure here.

Figure 6. The effect on transmembrane channel pore of ORF3a viroporin due to p.Q57H mutation. (a) The wild (Q_{57}) and mutant (H_{57}) ORF3a protein are presented in light gray and green color, respectively. The structural superposition displays no overall conformation change, however the histidine at 57 position of mutant ORF3a (deep blue) has slightly rotated from glutamine at same position of the wild protein (bright red). This change in rotamer state at 57 residue may influence **(b)** the overall stability of H_{57} (upper part) over Q_{57} (lower part) because of ionic interaction of histidine (green; stick model) of transmembrane domain 1 (TM1) with cysteine at 81 (yellow stick) of TM2. The color code defined different bond types is shown in inlet.

Figure 7. Structural superposition of wild and mutant N protein. The light grey color represents both wild ($RG_{203\text{-}204}$) and mutant ($KR_{203\text{-}204}$) N protein. The linker region (LKR: 183-247 amino acids) of wild ($RG_{203\text{-}204}$) and mutant ($KR_{203\text{-}204}$) are in pale yellow and warm pink color, respectively. **(a)** The aligned structures showed a highly destabilizing (Table 3) conformational change from 231 to 247 amino acids within LKR. Other regions of the N protein, especially the SR-rich region (184-204 amino acids) where the mutations occur, do

not change. **(b)** A more emphasized look into the SR-rich and mutated sites (RG203-204KR) of wild and mutant N protein represent slight deviation in the Ser (197) and Thr (198) while only glycine (green) to arginine (blue) substitution at 204 position shows changing at rotamer state. The enlarged view is shown in the bottom part.

.

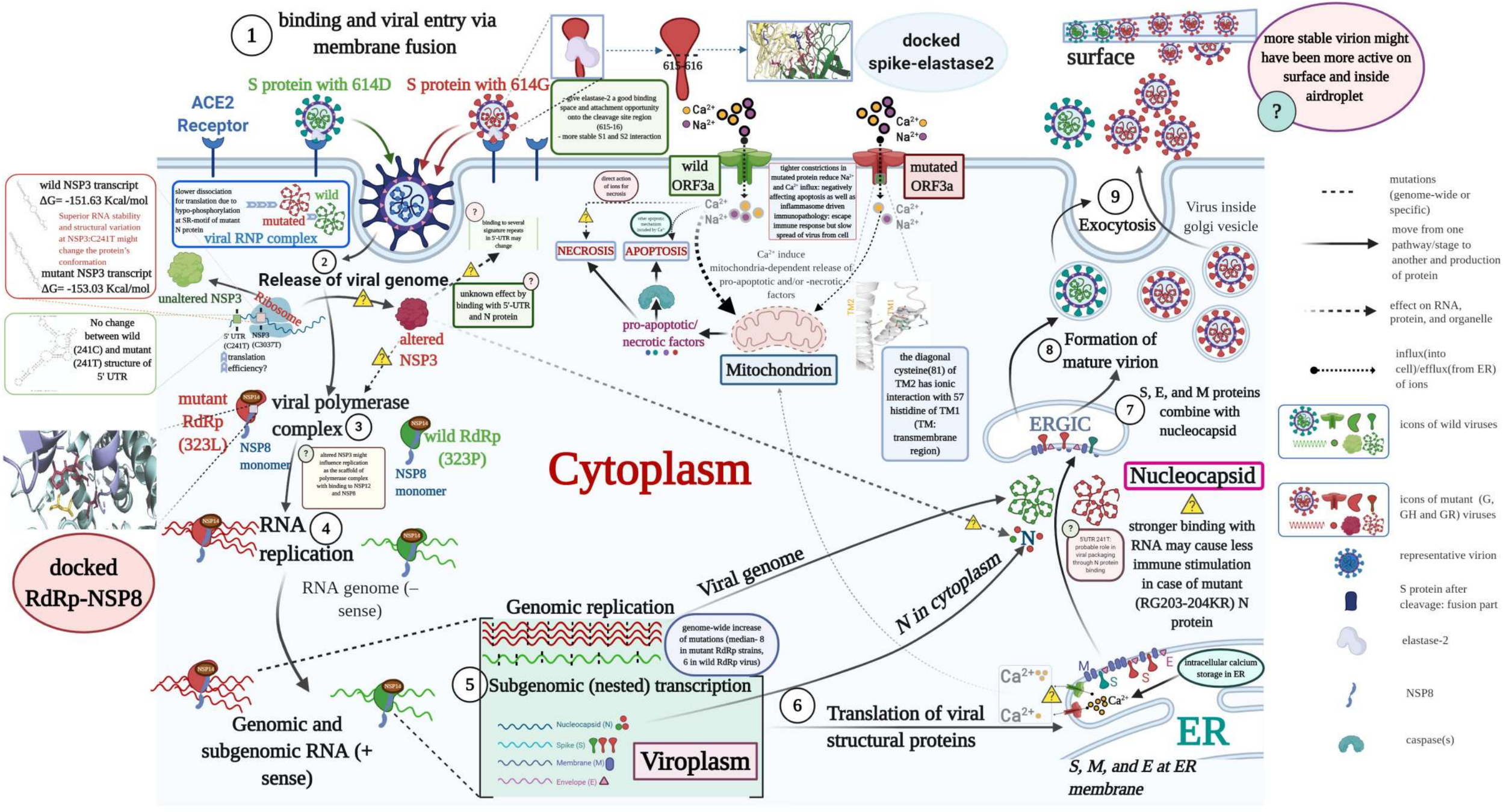
1 binding and viral entry via membrane fusion
S protein with 614D
S protein with 614G
ACE2 Receptor
615-616
docked spike-elastase2
give elastase-2 a good binding space and attachment opportunity onto the cleavage site region (615-16)
- more stable S1 and S2 interaction
surface
more stable virion might have been more active on surface and inside airdroplet
wild NSP3 transcript
ΔG= -151.63 Kcal/mol
Superior RNA stability and structural variation at NSP3:C241T might change the protein's conformation
mutant NSP3 transcript
ΔG= -153.03 Kcal/mol
No change between wild (241C) and mutant (241T) structure of 5' UTR
slower dissociation for translation due to hypo-phosphorylation at SR-motif of mutant N protein
wild
mutated
viral RNP complex
2 Release of viral genome
unaltered NSP3
Ribosome
5' UTR (C241T)
NSP3 (C3037T)
translation efficiency?
altered NSP3
binding to several signature repeats in 5'-UTR may change
unknown effect by binding with 5'-UTR and N protein
wild ORF3a
mutated ORF3a
tighter constrictions in mutated protein reduce Na2+ and Ca2+ influx: negatively affecting apoptosis as well as inflammasome driven immunopathology: escape immune response but slow spread of virus from cell
direct action of ions for necrosis
other apoptotic mechanism incuded by Ca2+
NECROSIS
APOPTOSIS
Ca2+ induce mitochondria-dependent release of pro-apoptotic and/or -necrotic factors
pro-apoptotic/ necrotic factors
Mitochondrion
TM2
TM1
the diagonal cysteine(81) of TM2 has ionic interaction with 57 histidine of TM1 (TM: transmembrane region)
9 Exocytosis
Virus inside golgi vesicle
8 Formation of mature virion
7 S, E, and M proteins combine with nucleocapsid
ERGIC
mutant RdRp (323L)
NSP14
NSP8 monomer
viral polymerase complex 3
wild RdRp (323P)
NSP8 monomer
altered NSP3 might influence replication as the scaffold of polymerase complex with binding to NSP12 and NSP8
Cytoplasm
docked RdRp-NSP8
RNA replication 4
RNA genome (– sense)
Viral genome
N in cytoplasm
N
Nucleocapsid
stronger binding with RNA may cause less immune stimulation in case of mutant (RG203-204KR) N protein
5'UTR 241T: probable role in viral packaging through N protein binding
Genomic replication
genome-wide increase of mutations (median- 8 in mutant RdRp strains, 6 in wild RdRp virus)
5 Subgenomic (nested) transcription
Nucleocapsid (N)
Spike (S)
Membrane (M)
Envelope (E)
Viroplasm
6 Translation of viral structural proteins
Genomic and subgenomic RNA (+ sense)
intracellular calcium storage in ER
ER
S, M, and E at ER membrane
mutations (genome-wide or specific)
move from one pathway/stage to another and production of protein
effect on RNA, protein, and organelle
influx(into cell)/efflux(from ER) of ions
icons of wild viruses
icons of mutant (G, GH and GR) viruses
representative virion
S protein after cleavage: fusion part
elastase-2
NSP8
caspase(s)

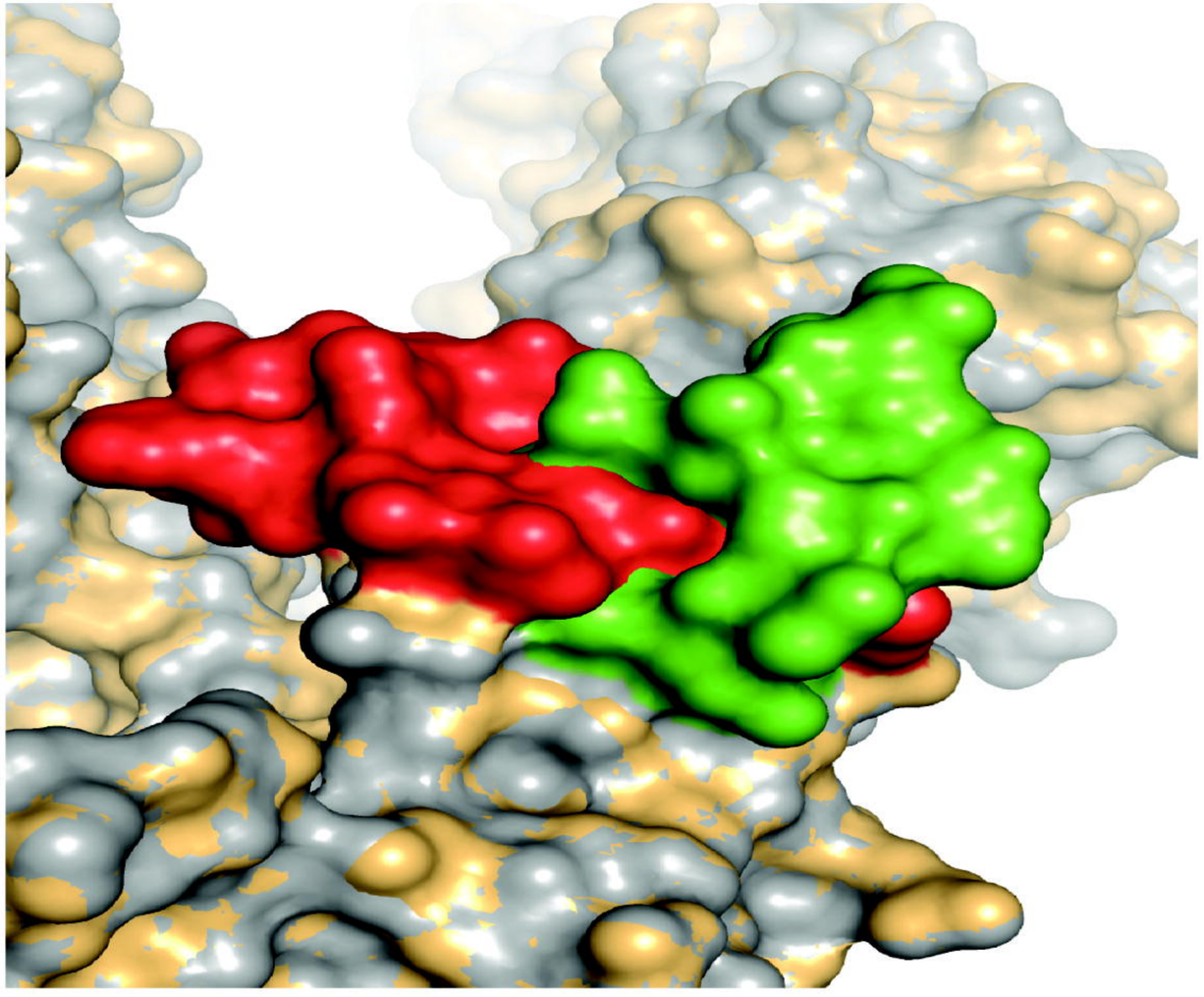

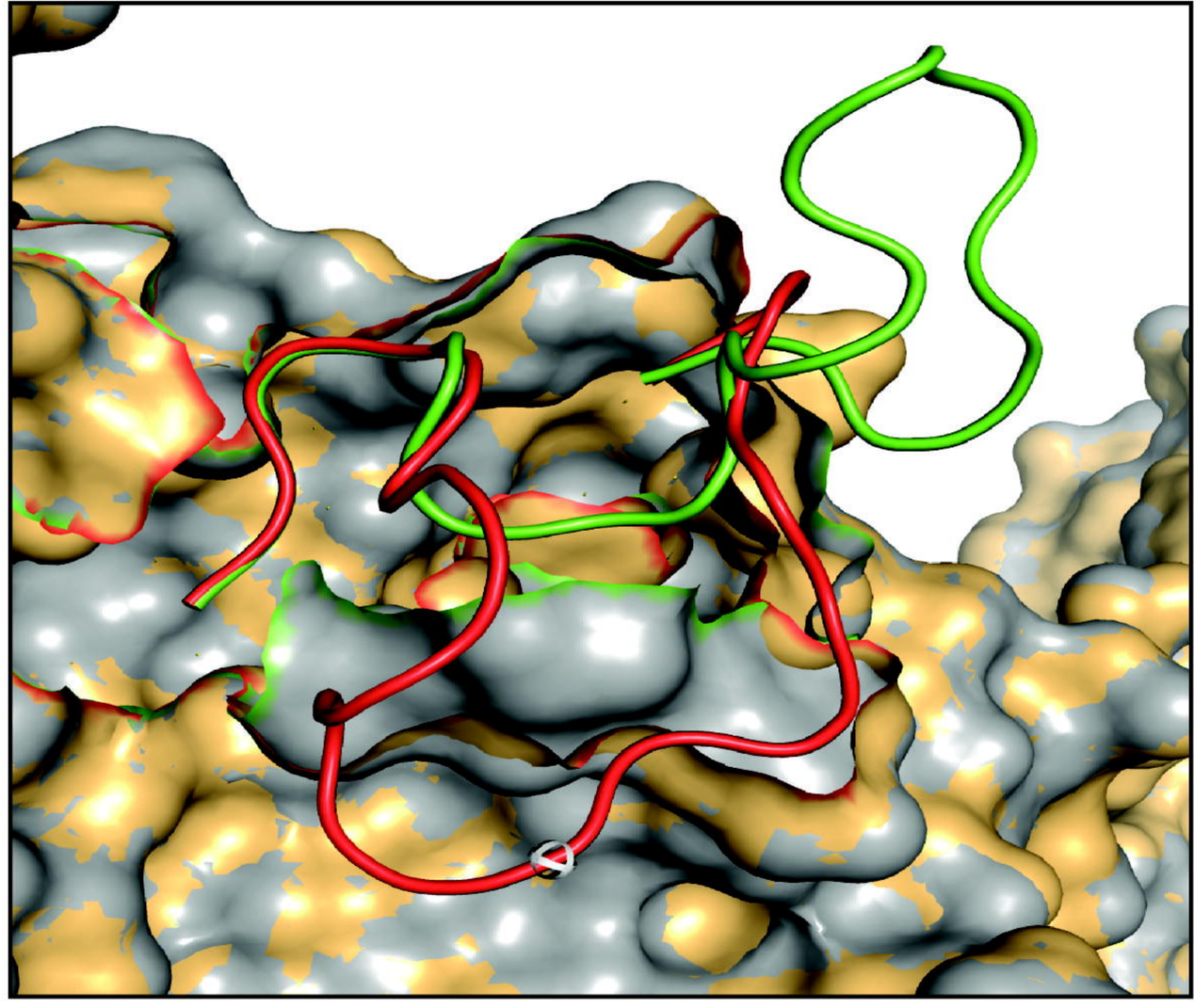

a

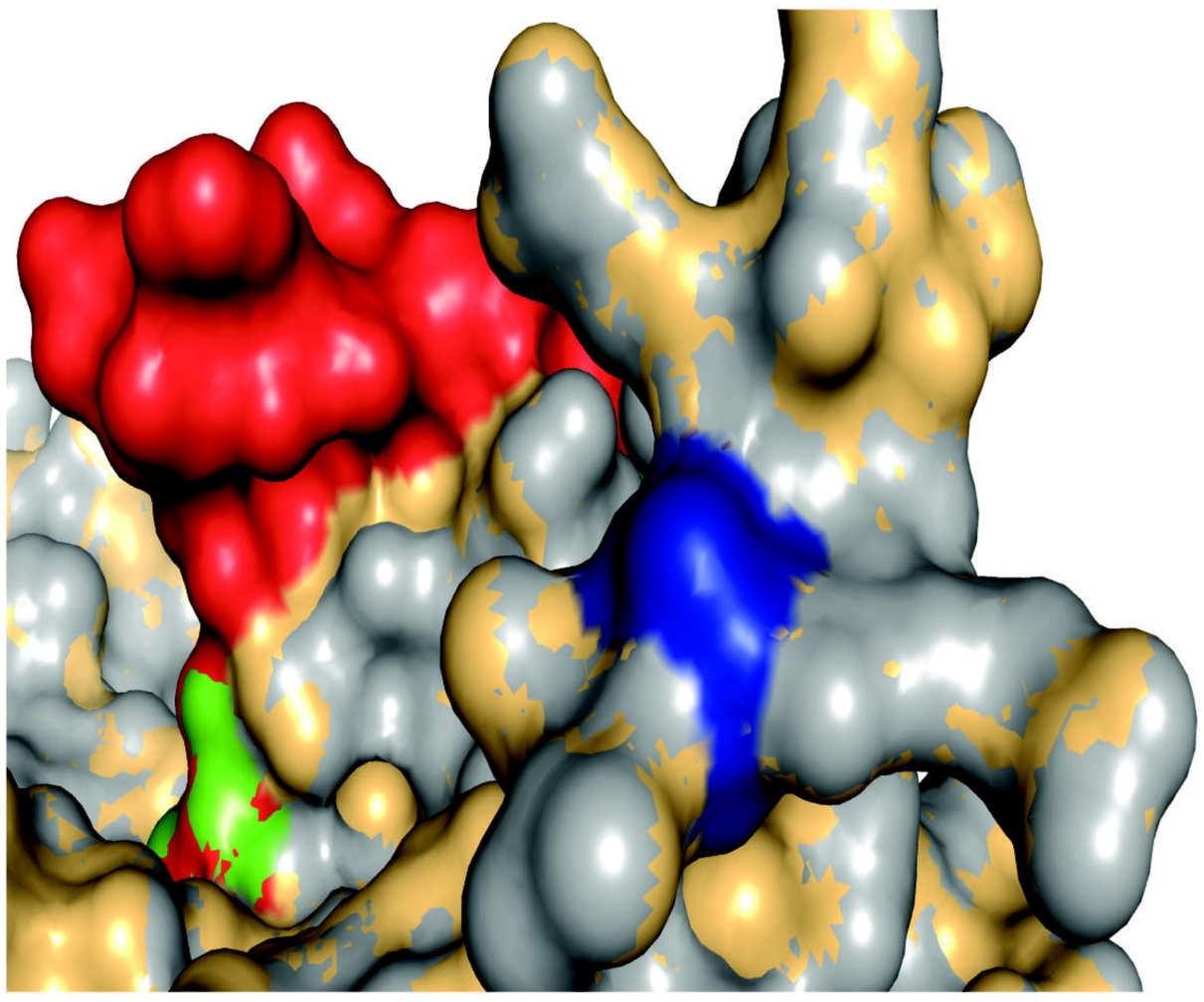

b

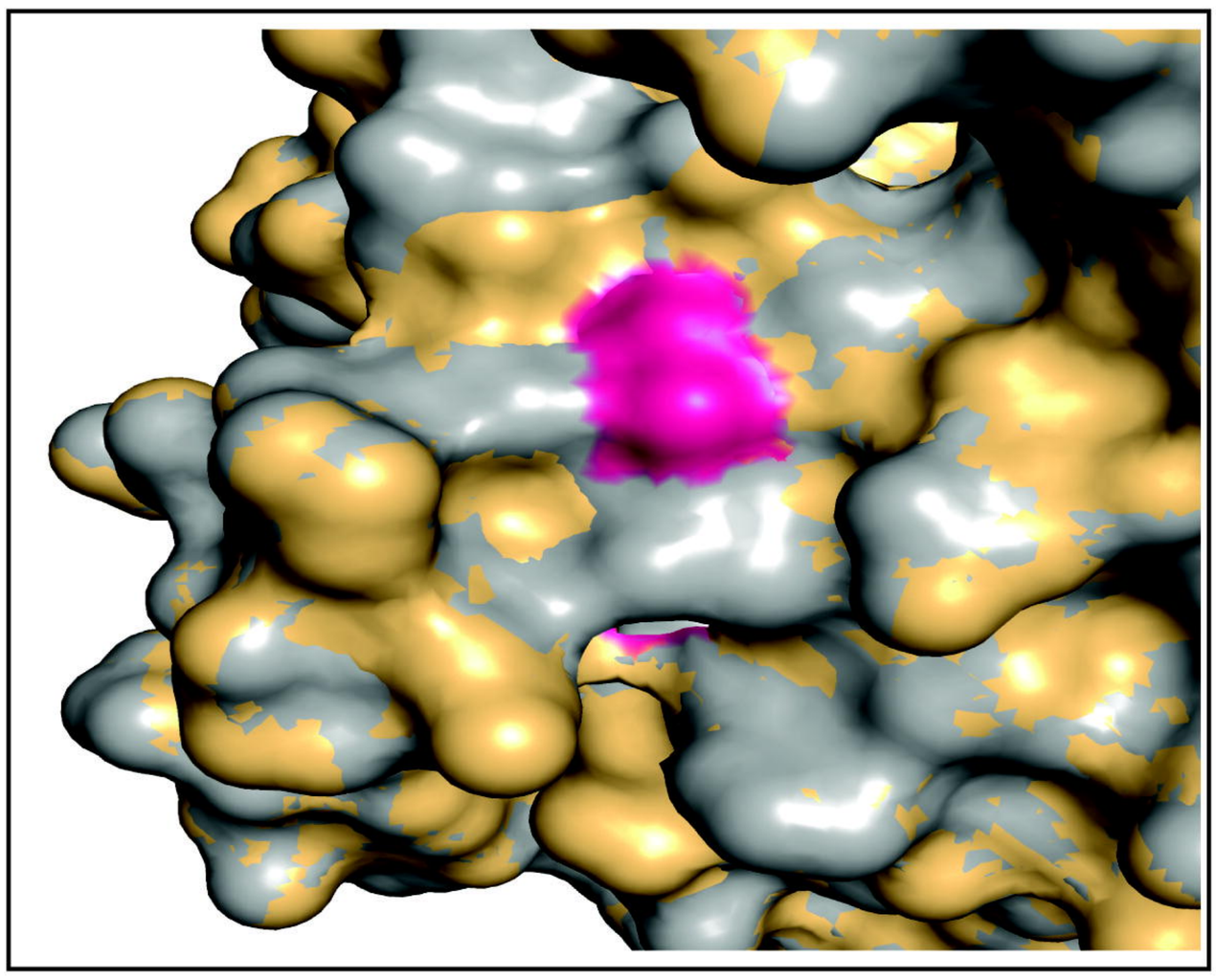

c

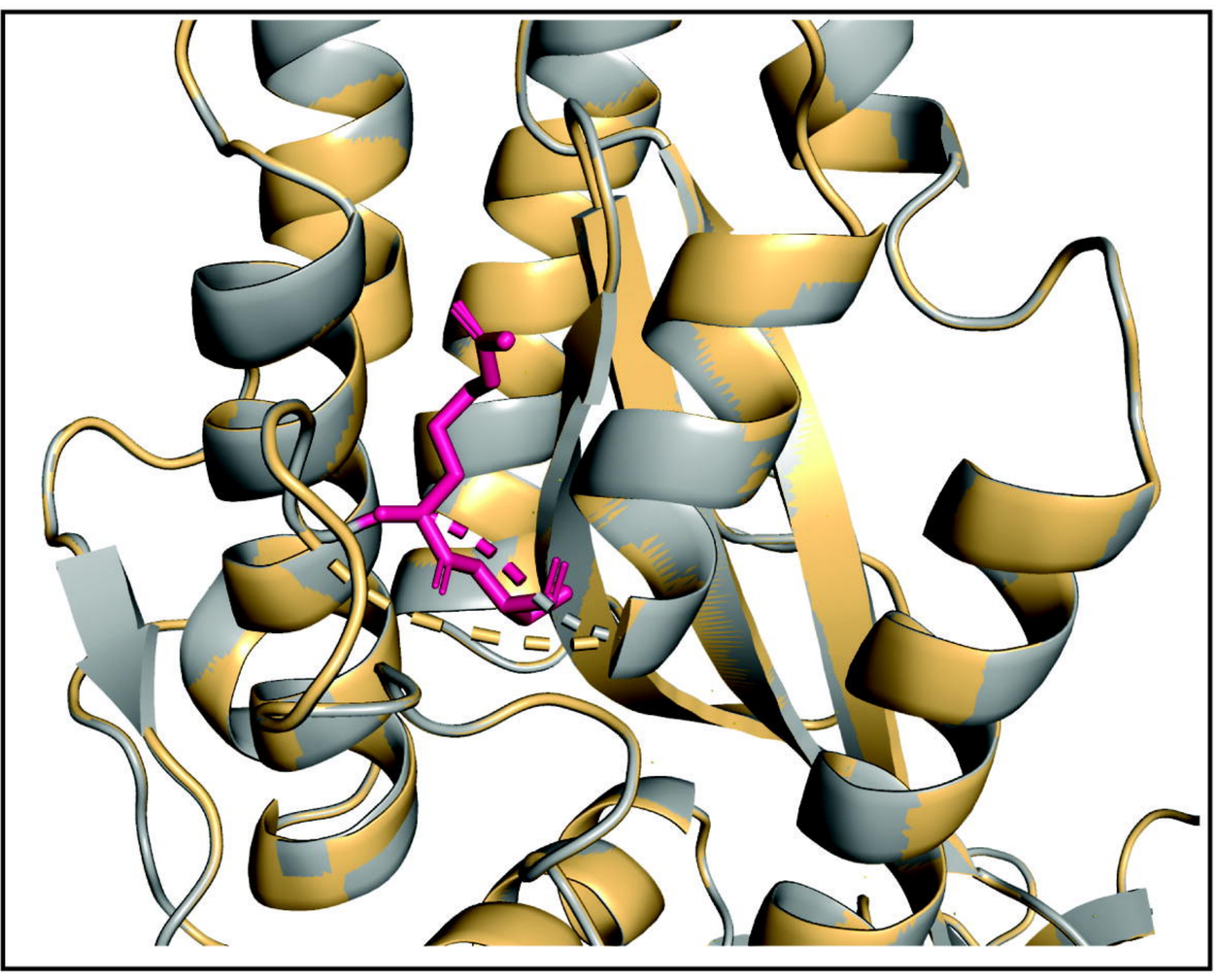

d

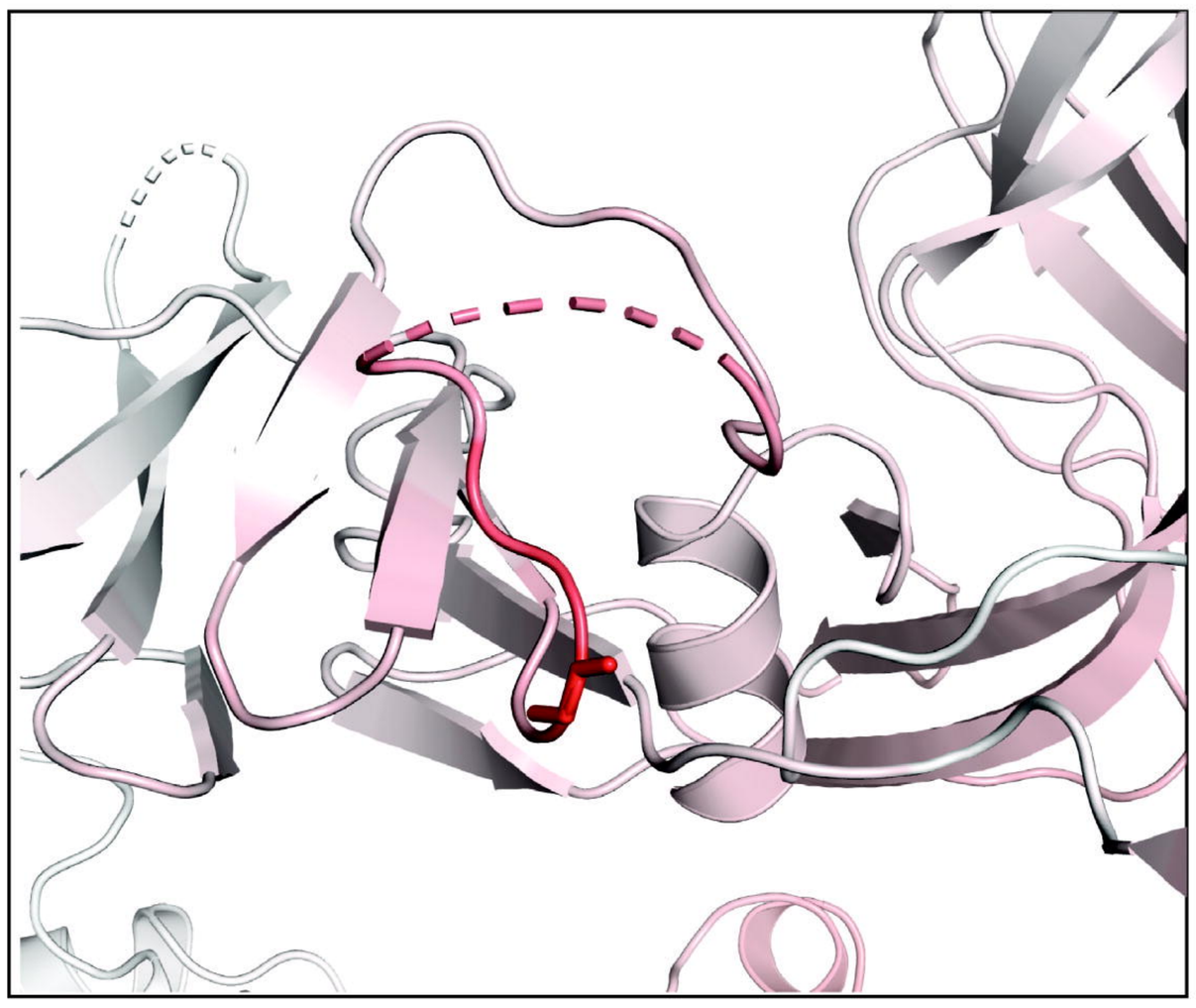

e

f

g

h

wild (D614) version of spike protein

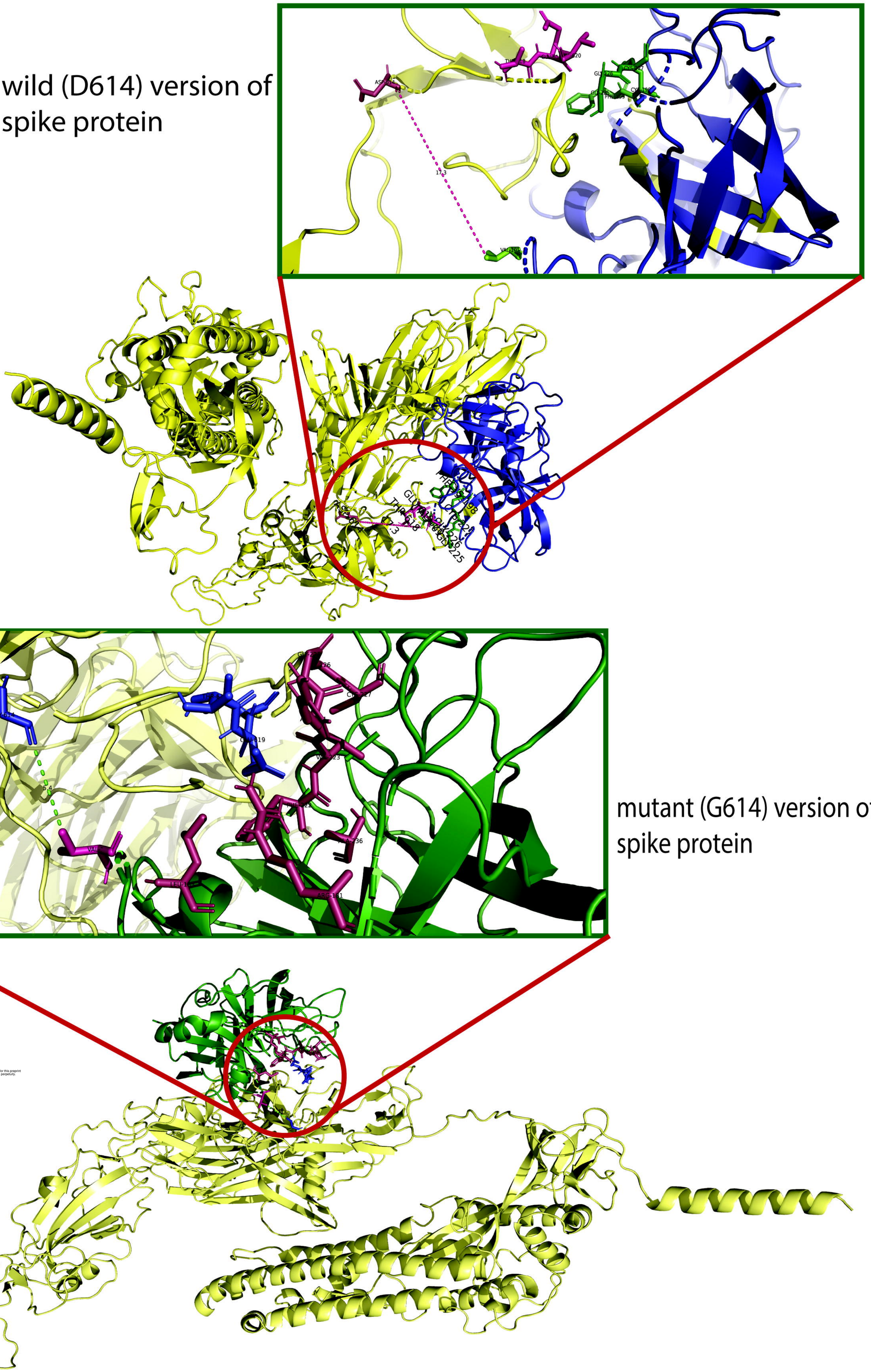

mutant (G614) version of spike protein

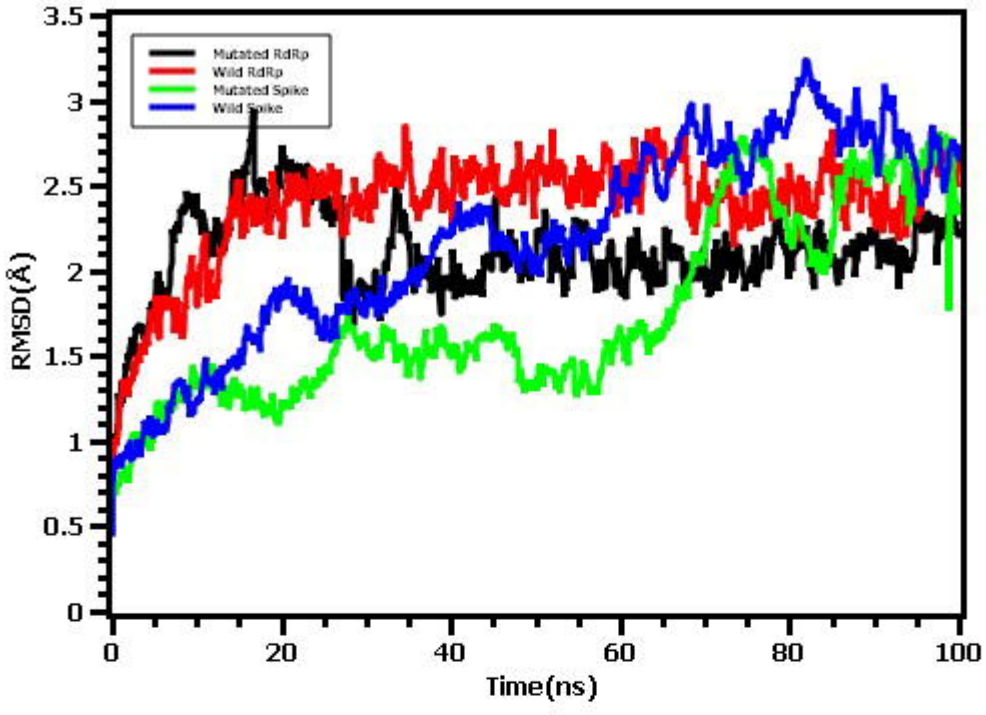

(a)

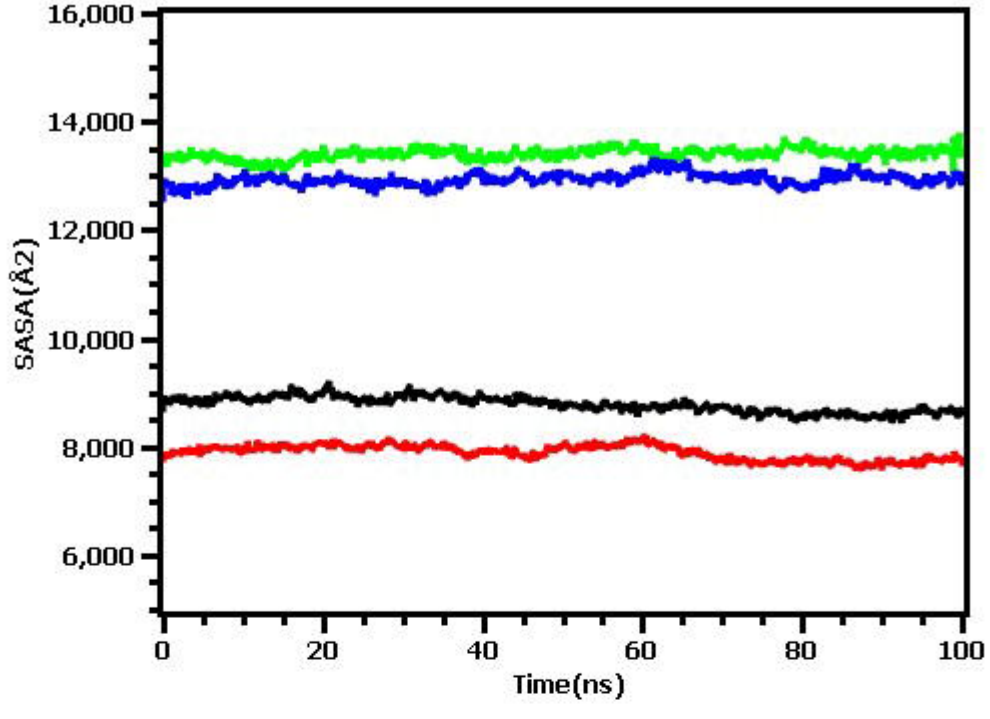

(b)

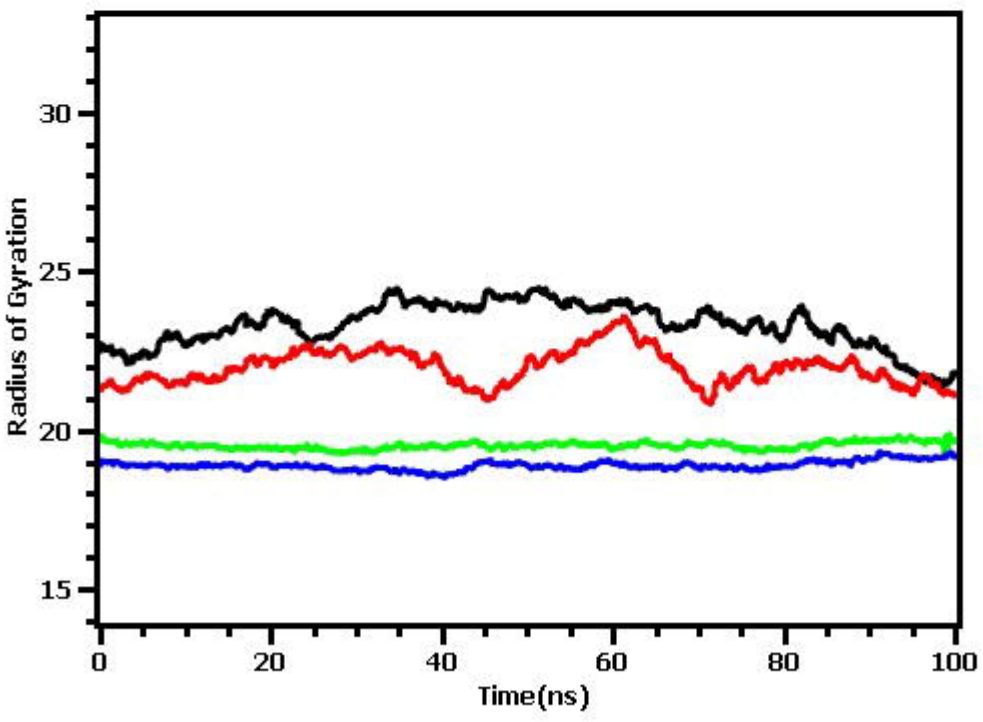

(c)

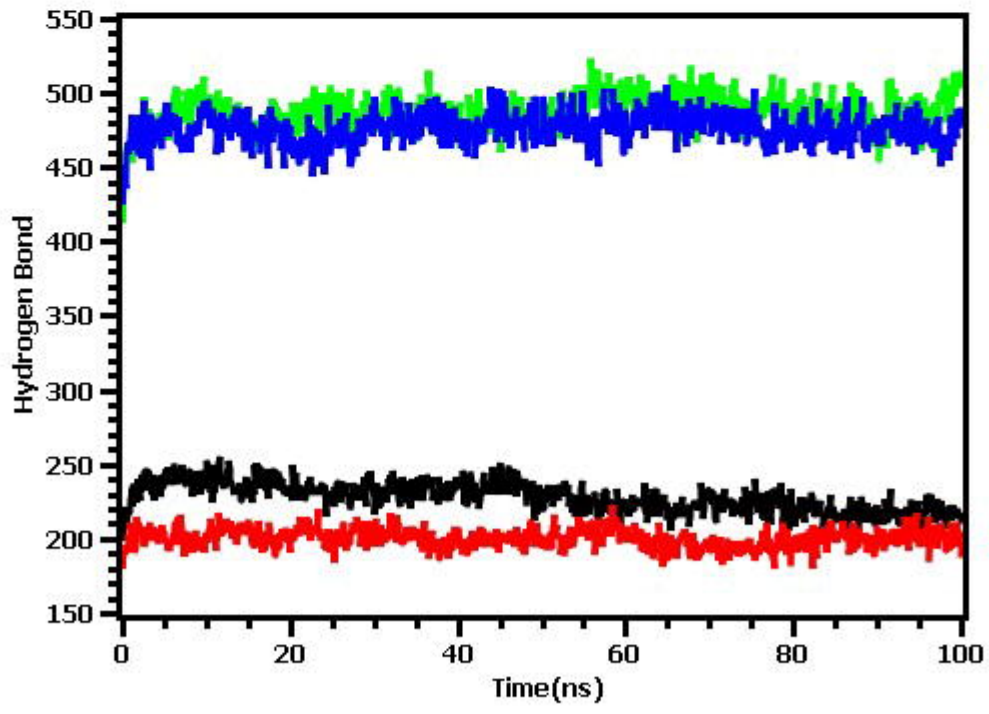

(d)

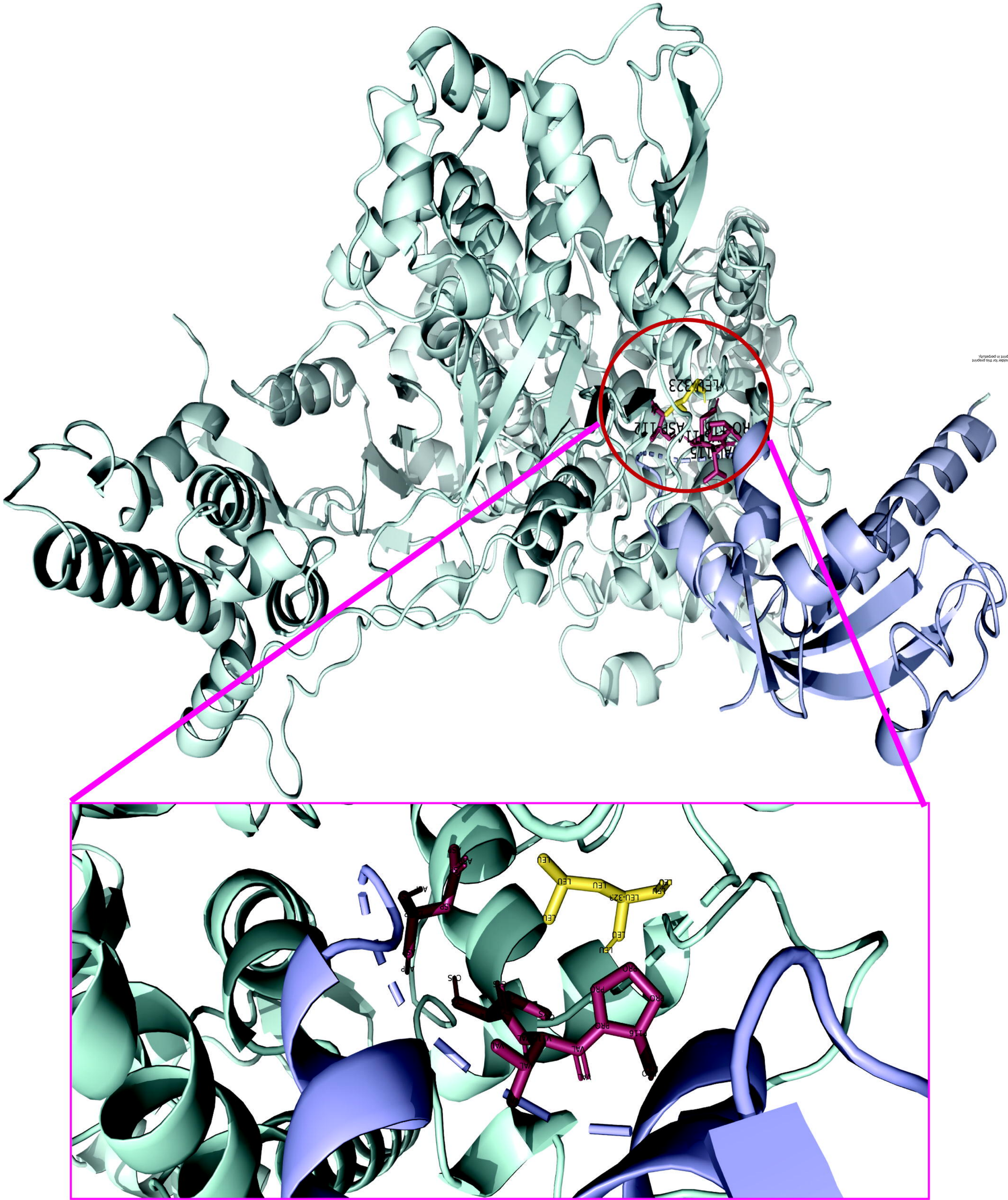

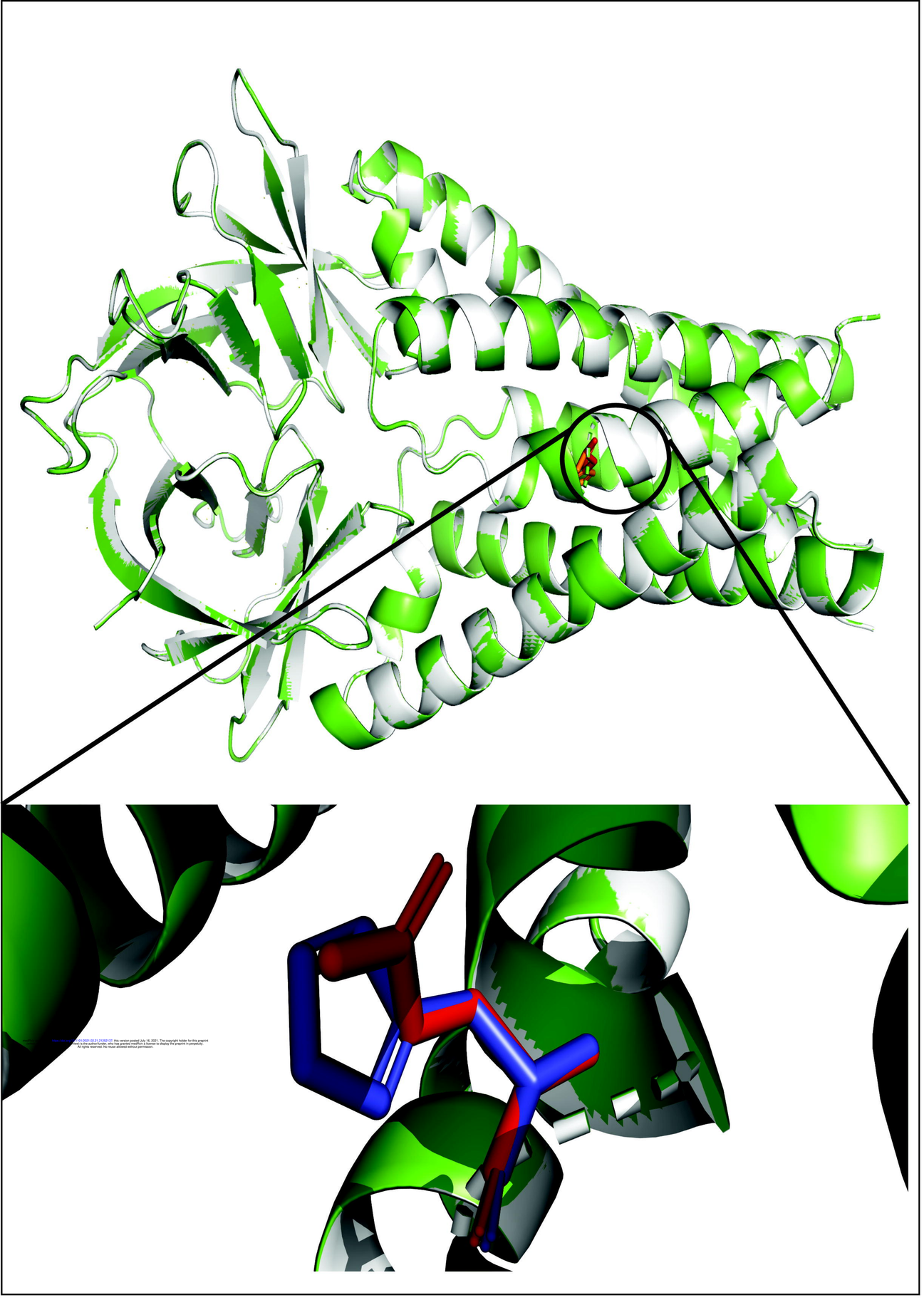

a

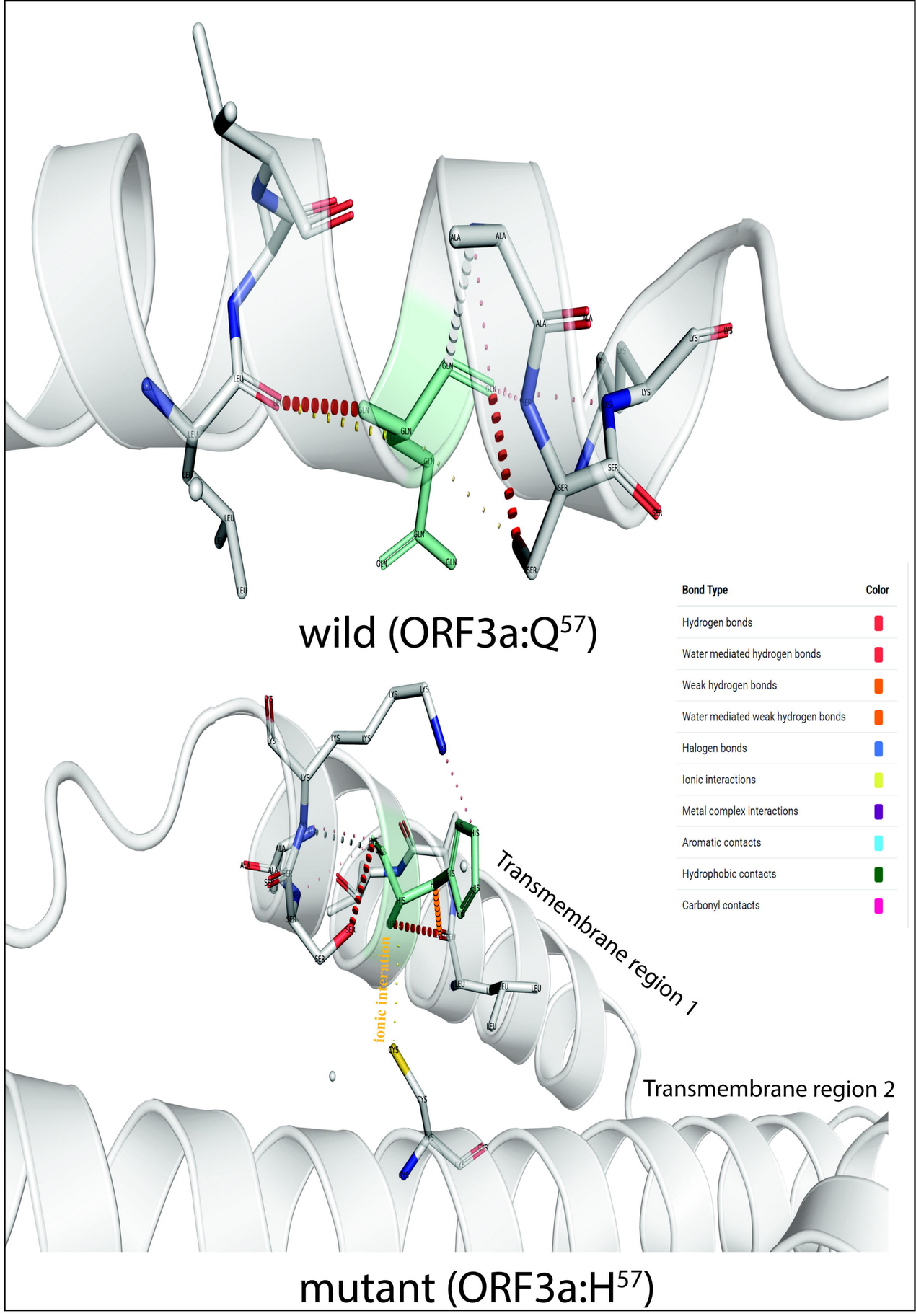
wild (ORF3a:Q57)
Bond Type
Color
Hydrogen bonds
Water mediated hydrogen bonds
Weak hydrogen bonds
Water mediated weak hydrogen bonds
Halogen bonds
Ionic interactions
Metal complex interactions
Aromatic contacts
Hydrophobic contacts
Carbonyl contacts
Transmembrane region 1
ionic interaction
Transmembrane region 2
mutant (ORF3a:H57)

b

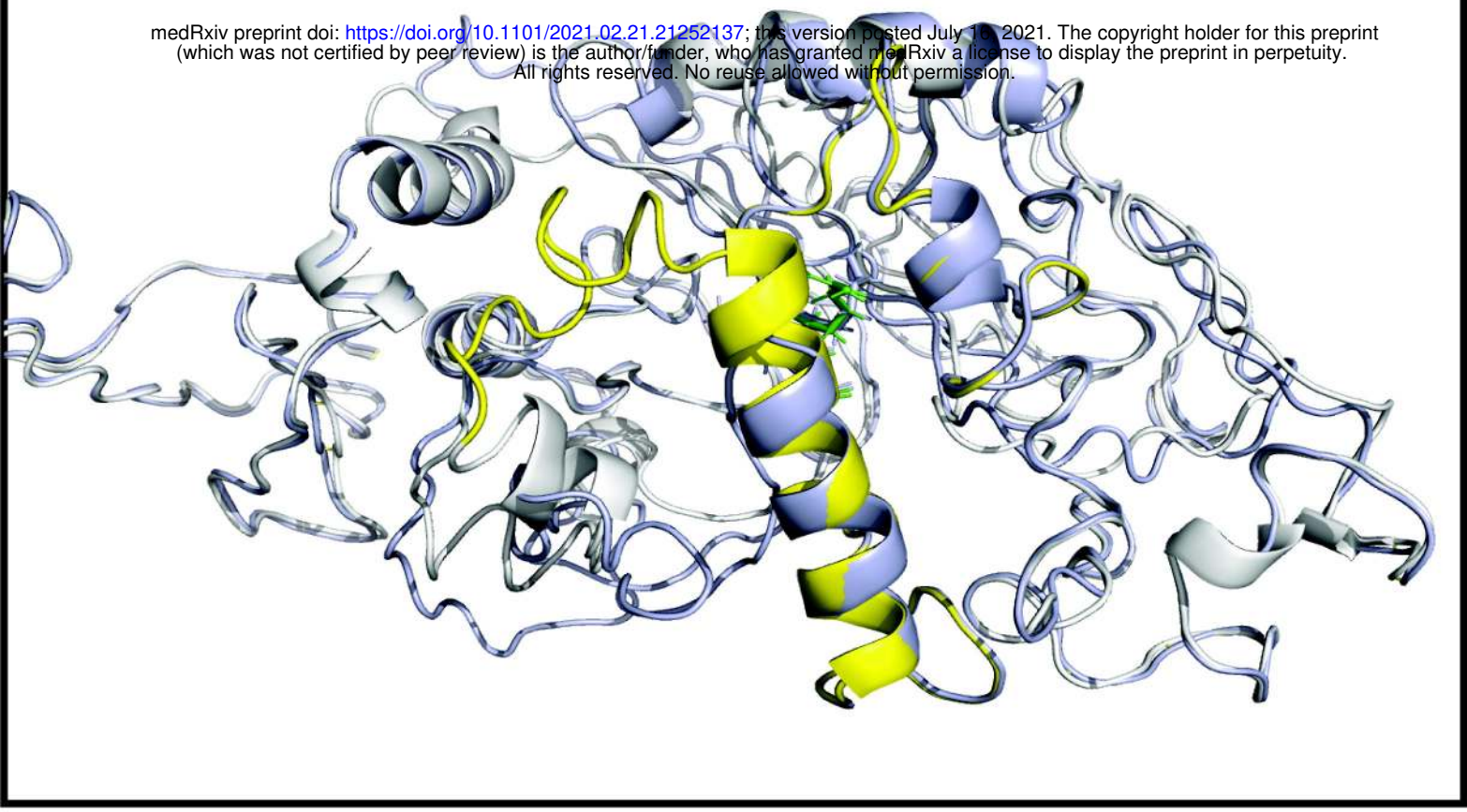

a

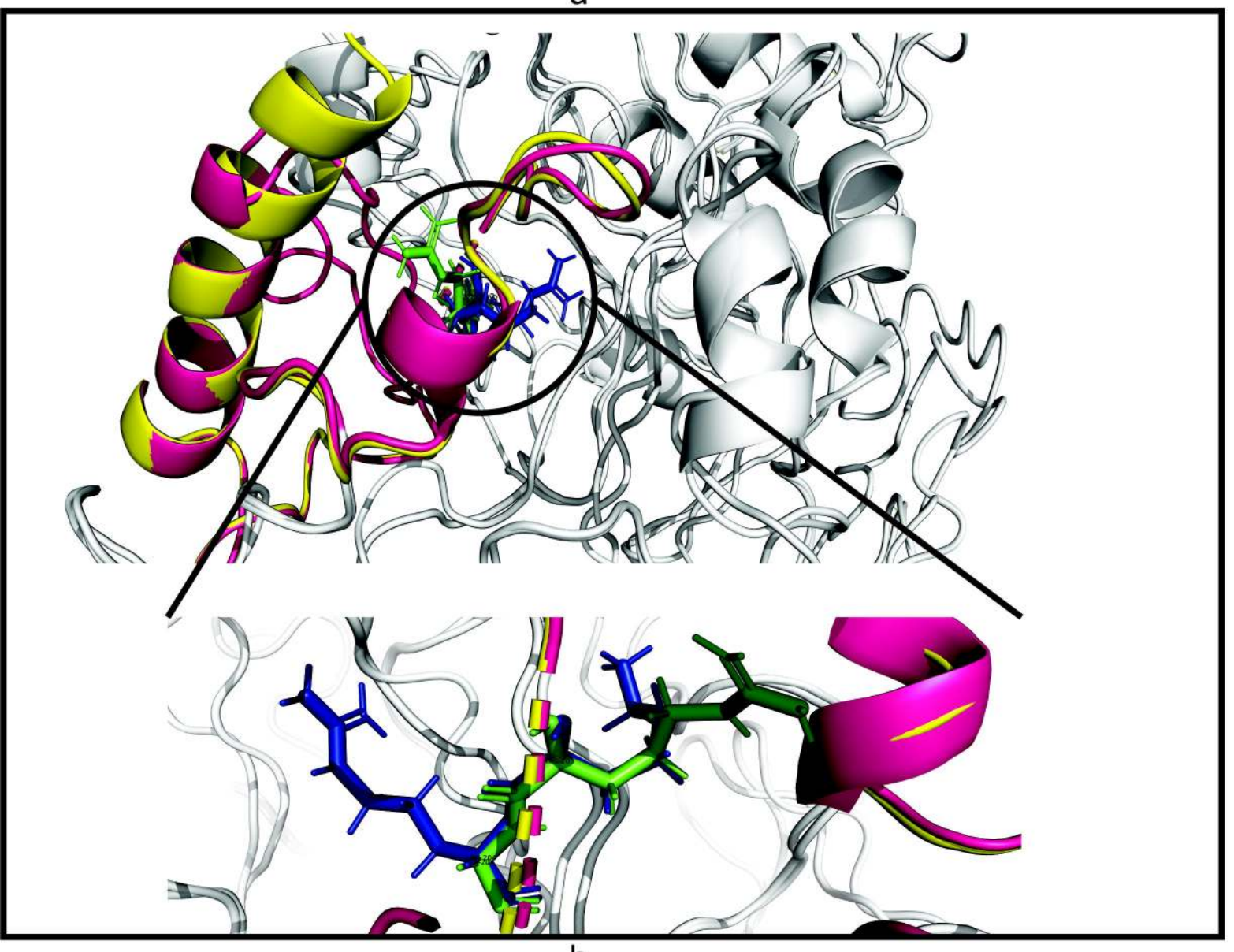

b